Measuring the 5D Excited Energy Levels of Rubidium Atoms Using Laser Spectroscopy

A thesis submitted in partial fulfillment of the requirement
for the degree of Bachelor of Science with Honors in
Physics from the College of William and Mary in Virginia,

by

Mia P. Bridges

Advisor: Prof. Seth Aubin

Prof. S. Mordijck

Prof. R. Iaci

Williamsburg, Virginia
May 1 2025

Contents

Acknowledgments **iii**

List of Figures **v**

List of Tables **vi**

Abstract **i**

1 Introduction **1**

1.1 Motivations 1

1.2 Research Summary 4

1.3 Thesis Structure 6

2 Theory **7**

2.1 Quantum Theory of Absorption & Fluorescence Spectroscopy 7

2.2 Laser Absorption Spectroscopy:

Doppler Broadened & Saturation Spectroscopy 8

2.3 Electromagnetically-Induced Transparency 11

3 Methods **13**

3.1 Basics of Spectroscopy 13

3.1.1 5S Levels: Fluorescence & Doppler Broadened Absorption Spectroscopy . . . 13
3.1.2 5P Levels: Laser Saturated Absorption Spectroscopy & Ground State EIT . . . 16
3.2 Measuring the 5D Levels . . . 23
3.2.1 5D Fluorescence Spectroscopy in Vapor Cell . . . 23
3.2.2 5D Fluorescence in the Cold Atom Apparatus . . . 30

4 Results and Analysis **31**
4.1 5D Fluorescence in Vapor Cell . . . 31
4.1.1 Error Analysis . . . 38
4.2 5D Fluorescence in Cold Atom Apparatus . . . 41

5 Conclusion & Next Steps **44**

References **46**

Acknowledgments

I would like to thank Dr. Seth Aubin for his continuous support through this thesis, as well as in my time at William & Mary as a whole. Without his guidance, my achievements in this work would not have been possible. I would also like to thank the members of the Aubin lab for their guidance and assistance with this project, including graduate students William Miyahira, Trevor Tingle, and Russell Kamback, and undergrads Sarah Sasinowska and Valo Dandashi, as well as Dr. Mykhailo Vorobiov from Dr. Irina Novikova's lab group. Additionally, I would like to thank Dr. Saskia Mordjick and Dr. Ross Iaci for being on my thesis committee and providing help and feedback on my thesis. Finally, I would like to thank my friends and family for all of their support through the past four years and beyond. I truly would not have been able to do it without you.

List of Figures

1.1 Rubidium energy level diagram 2

1.2 Rubidium energy level diagram with excitation directly from 5P to Rydberg levels 3

2.1 Absorption vs. fluorescence spectroscopy diagram 9

2.2 Doppler effect diagram 10

2.3 Electromagnetically induced transparency diagram 12

3.1 Doppler broadened spectroscopy setup diagram 14

3.2 5P to 5S Fluorescence 14

3.3 Doppler broadened spectroscopy graph 15

3.4 Saturation spectroscopy setup diagram 17

3.5 Doppler broadened vs. saturation spectroscopy data 18

3.6 Rubidium 87 saturation spectroscopy graph 19

3.7 Rubidium 85 saturation spectroscopy graph 20

3.8 Ground state EIT setup diagram 21

3.9 Ground state EIT, increased absorption 22

3.10 Ground state EIT, decreased absorption 22

3.11 Fluorescence spectroscopy setup diagram 25

3.12 PMT stand 26

3.13 Laser Pedestal Diagram 28

3.14 Second 5D Fluorescence Setup 29
3.15 Magneto-Optical Trap 30

4.1 Initial fluorescence spectroscopy data 32
4.2 Fluorescence spectroscopy data 33
4.3 Vapor cell rotation 33
4.4 Data from straight vs rotated vapor cell 34
4.5 Piezo Voltage to Wavelength Calibration Fit 35
4.6 5D fluorescence spectroscopy graph on frequency scale 36
4.7 ^{85}Rb 5D fluorescence spectrum with full background 38
4.8 ^{85}Rb 5D fluorescence spectrum with residuals 40
4.9 MOT fluorescence 41
4.10 Photopeak graph and fluorescence data from fluorescence spectroscopy in MOT 42

List of Tables

1.1 $5P \rightarrow 5D$ resonant transition wavelengths 5

1.2 ^{85}Rb and ^{87}Rb $5D_{5/2}$ hyperfine structure splittings 5

3.1 $5S_{1/2}$ Hyperfine Splittings 16

3.2 ^{87}Rb $5P_{3/2}$ Hyperfine Splittings 19

3.3 ^{85}Rb $5P_{3/2}$ Hyperfine Splittings 20

4.1 5D hyperfine splittings, averaged from two methods of errorbar generation 41

Abstract

The valence electron of a rubidium atom can be excited from the 5D level to the Rydberg levels, including the nP levels and the "n" Stark manifold (e.g. n=50), via a third photon. In the Rydberg levels, atoms are very sensitive to external electric fields, and the energy-level shift observed can be used to measure the applied electric field that caused it. This phenomenon can be applied to an ongoing project on non-invasive electron beam imaging using rubidium atoms, as the electric field of the electrons will impact the energy levels of the atoms in the Rydberg levels. This project consists of the excitation, detection, and measurement of the 5D energy levels of rubidium using laser spectroscopy with two lasers at 780 nm and 776 nm, which one must first excite through in order to reach the Rydberg levels. The excitation process involves shooting a 780 nm laser through a cloud of rubidium atoms to excite them to the $5P_{3/2}$ level, then using a 776 nm laser to excite the atoms to the $5D_{5/2}$ states. The 5D energy levels are then detected and measured via the resulting emission spectrum, including detecting their decay to the $5S_{1/2}$ ground state at 420 nm through the 6P states. This process is completed in a vapor cell and a cold atom apparatus.

Chapter 1

Introduction

1.1 Motivations

The College of William & Mary's Physics department and Jefferson Lab are currently collaborating on an ongoing project concerning noninvasive imaging of electron beams and charged particle tracks. Typically, to detect electrons and other charged particles, one must intercept or impact them, invasively altering their trajectory. This process is not ideal for some experiments, where a person might prefer to observe charged particles in their original trajectory and have them continue unimpeded towards an experiment. Thus, it is important to determine a noninvasive method of observing charged particles.

A current idea for how to achieve this goal is to utilize the Stark manifold of rubidium atoms. The Stark manifold is the name for the collective Rydberg energy levels of rubidium, which are states with high angular momentum (typically above nD) (see Figure 1.1). The Stark manifold is significant because the energy levels within it are all effectively degenerate with each other, which makes them more sensitive to the Stark effect.

The Stark effect is a phenomenon in which an atom's spectral lines shift in the presence of an external electric field. It normally must be calculated using second

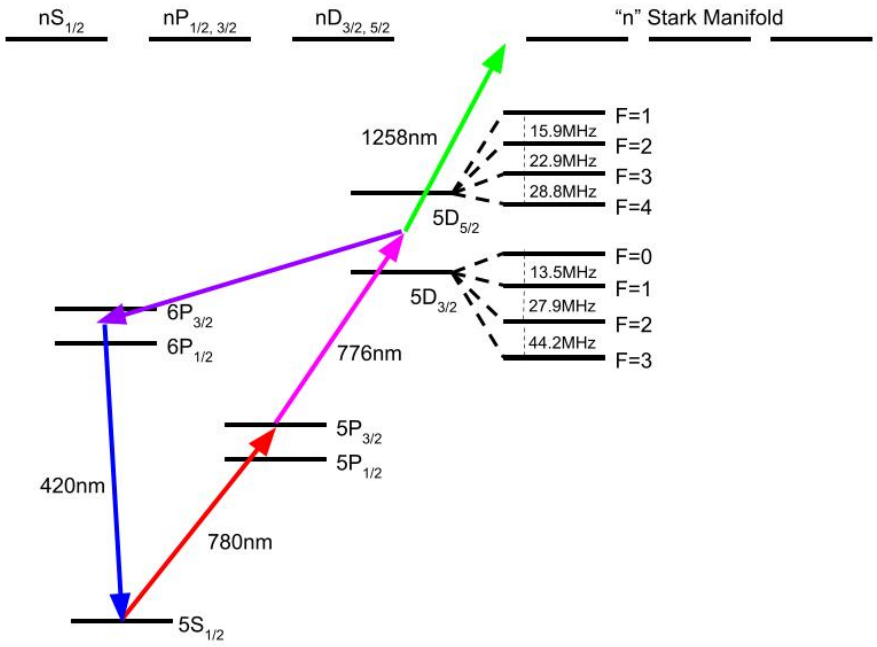

Figure 1.1: Diagram of relevant energy levels of ^{87}Rb, adapted from [1]. 5D splittings are approximate and obtained from [2].

order perturbation theory; however, in the Stark manifold, it can be calculated using first order perturbation theory due to the degeneracy of the energy levels. This means that atoms in the Stark manifold will experience a linear Stark effect as opposed to a quadratic one; thus, they are much more sensitive to small changes in electric fields than atoms in other energy levels.

This extreme sensitivity to changes in electric fields is what could allow rubidium atoms in the Stark manifold to noninvasively image electron beams and other charged particle tracks. By shooting a beam of charged particles through a low-density cloud of rubidium atoms in the Stark manifold, one could observe the Stark effect caused by the electric fields these charged particles generate [3]. One could then calculate the movements of the charged particles utilizing the Stark effects they cause on the rubidium atoms. This method is a noninvasive procedure that would not involve

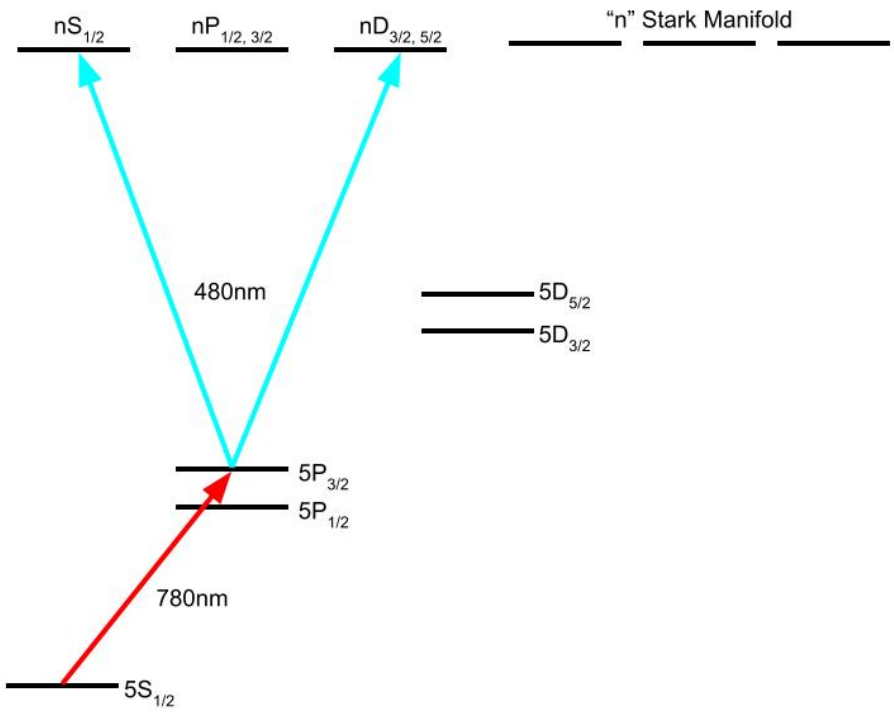

Figure 1.2: Diagram of energy levels of ^{87}Rb, showing two-step excitation process to Rydberg levels. Note that in the two-step process, the 5D levels are not excited through.

directly observing the charged particles themselves, but observing them through the Stark effect of the rubidium atoms. This would alleviate the concerns of altering the charged particle trajectories with direct observation.

In order to access the Rydberg levels, rubidium atoms must be excited in either a three-step process from the 5S levels through the 5P and 5D levels (as in Figure 1.1), or a two-step process from the 5S levels through the 5P levels and directly up to the Rydberg levels (see Figure 1.2) [4]. This project focuses on the three-step transition method, as the two-step transition method has been attempted and is not ideal. The two-step method of excitation induces a photoelectric effect [5], which is when a surface absorbs the energy from a photon and subsequently emits an electron.

This occurs more in the two-step excitation method because the laser needed to excite rubidium from the 5P to Rydberg levels is a 480 nm laser [4], which has a shorter wavelength, higher frequency, and greater energy than the longer wavelength lasers used in the three-step process. Comparatively, excitation from the 5P to Rydberg levels in the three-step process is done with 776 and 1258 nm lasers, which are much less likely to generate a photoelectric effect due to their longer wavelength. The electrons generated by the photoelectric effect cause difficulty when one is trying to detect very small changes in the electric field caused by external electrons and other charged particles, as it is difficult to distinguish between external charged particles and the photo-electrons generated by the lasers used to excite it. A change in electric field caused by the laser itself causes inaccuracy when ultimately trying to observe the Stark effect.

In order to efficiently excite rubidium atoms to the Rydberg levels and measure changes in the observed Stark effect once there, we must know the precise values for the energy transitions between levels. It is also helpful to know the hyperfine structure of each transition level that the rubidium goes through on its way to the Rydberg levels. The hyperfine structure is the name for the minute separations between spectral lines within certain energy levels, and is caused by quantum interactions between the spins of the nucleus and the valence electron within atoms [6]. This project focuses on the transition to the 5D level and its hyperfine structure specifically, as the transitions and hyperfine structure of the 5P levels are already well known.

1.2 Research Summary

The specific objective of this thesis was to measure the wavelength of laser needed to excite from the 5P levels to 5D levels of rubidium, as well as the hyperfine structure of rubidium's 5D levels. Rubidium naturally has two isotopes: rubidium-87

(^{87}Rb) and rubidium-85 (^{85}Rb). Additionally, rubidium has two 5D fine structure levels: the $5D_{3/2}$ level and the $5D_{5/2}$ level. This research focused on observing the transition to and hyperfine splittings of the $5D_{5/2}$ level in ^{87}Rb and ^{85}Rb. The ultimate goal of this research was to obtain the most precise values for the transition and hyperfine splittings as possible.

The 5D energy levels and hyperfine structure were measured using fluorescence spectroscopy. Using this method, this thesis was successful in identifying and measuring the wavelength transition value to the $5D_{5/2}$ level (Table 1.1). By fitting the fluorescence spectroscopy data, this research also successfully observed and obtained values for the hyperfine splittings of the $5D_{5/2}$ levels for both rubidium-85 and rubidium-87 (Table 1.2), although more work is needed to verify their accuracy. These results are shown in the tables below and are elaborated upon in subsequent chapters:

5D Transition	Resonant Frequency (nm)
$5D_{5/2}$	775.9776 ± 0.0001 nm

Table 1.1: Resonant wavelengths for 5P to 5D transitions of rubidium in nanometers, determined by fluorescence spectroscopy. Error is statistical.

Observed $5D_{5/2}$ Splitting Frequencies (MHz)			
Rubidium-85		Rubidium-87	
Peak A $\rightarrow$ Peak B	31.0 $\pm$ 4.7 MHz	F=2 $\rightarrow$ F=3	34.6 $\pm$ 75.8* MHz
Peak B $\rightarrow$ Peak C	25.9 $\pm$ 22.2* MHz	F=3 $\rightarrow$ F=3	41.8 $\pm$ 196.6* MHz

Table 1.2: Observed hyperfine structure splittings for $5D_{5/2}$ levels of rubidium-85 and rubidium-87 in megahertz. F levels for ^{85}Rb splittings are currently uncertain, and are instead labeled by Peaks A, B, and C. Starred error bars are larger than expected; more analysis and data are likely needed.

The fluorescence spectroscopy method will be discussed in more depth throughout this thesis. A further goal for this project was to measure the $5D_{5/2}$ levels with an ad-

ditional method known as electromagnetically-induced transparency (EIT). However, due to time constraints, this goal was not realized and has become a future objective for this project.

A secondary objective of this thesis was to measure the 5D levels in multiple different configurations of rubidium - namely, in both a vapor cell and a cold atom apparatus. The 5D levels were successfully observed in both configurations, achieving this goal. However, the energy levels observed in the cold atom apparatus were observed more qualitatively than quantitatively; obtaining a more quantitative measurement for the 5D levels in cold rubidium atoms remains a future goal.

1.3 Thesis Structure

This thesis is structured in the following manner: Chapter 2 covers the theory behind the multiple methods of spectroscopy used to measure the energy levels of rubidium in this experiment. Chapter 3 details the specific methods taken to spectroscopically measure the energy levels of rubidium and contains two main sections. The first section provides methods for measuring the 5S and 5P levels of rubidium, as these levels must be known in order to excite to the 5D levels, and the methods used in measuring them can be applied to the measurement of the 5D levels as well. The second section discusses the methods for measuring the 5D energy levels. Chapter 4 analyzes the results that came from measuring the 5D levels of rubidium, as well as enumerates the resonant frequency and wavelength values of the 5D levels and hyperfine structures. Chapter 5 summarizes these results and hypothesizes on the future of this project, as well as details the goals that could be achieved by future students taking on this research.

Chapter 2

Theory

This chapter explains the multiple spectroscopy methods used to measure the energy levels of rubidium in this experiment.

2.1 Quantum Theory of Absorption & Fluorescence Spectroscopy

Due to the discrete quantum numbers in their wavefunctions, electrons can only be found at certain distances from an atom's nucleus (proportional to quantum number n^2) [6]. Because it takes a specified amount of energy to move an election said distance farther away from the nucleus, these quantified distance levels are called energy levels. As the energy of a photon is proportional to its frequency, we can use photons of certain frequencies (and therefore, certain quantified energies) to excite atoms to different energy levels. This is the basis of spectroscopy.

Absorption spectroscopy is a method of determining energy transitions in an atom or molecule by observing changes in the spectrum of light after it is beamed through a vapor cloud of atoms. When the frequency of light matches the transition frequency of the atoms in vapor (called a resonant frequency), the atoms are excited and generate an absorption spectra. This can be observed when viewing a spectrum of the light after it passes through the atom vapor. A dark absorption line will occur at the

frequency corresponding to the energy of light that the atoms absorbed. This is how we can observe the exact frequencies of light that correspond to an energy level transition in an atom.

Fluorescence spectroscopy is intrinsically tied to absorption spectroscopy. When light at the resonant frequency passes though a cloud of atoms, they absorb the light's energy and excite to the above energy levels. However, soon after, the atoms will often de-excite and lose energy due to the upper energy levels being unstable states. When atoms de-excite, they lose energy in quantified amounts depending on the energy difference between the energy transitions, similarly to how they must gain quantified amounts of energy to excite to a new energy level. This loss of energy will cause de-exciting atoms to emit a photon of that specific energy, which corresponds to a set frequency. The cloud of atoms will glow with light of that specific frequency, which is how fluorescence spectroscopy can be observed. Fluorescence spectroscopy can be used to determine when incoming light's frequency is resonant in a cloud of atoms, as the atoms will then fluoresce. See Figure 2.1 for a simple illustration of the signals of absorption and fluorescence spectroscopy.

2.2 Laser Absorption Spectroscopy: Doppler Broadened & Saturation Spectroscopy

In laser absorption spectroscopy, a laser is passed through a cloud of atomic vapor, and the frequency is varied over time (known as "scanning" the laser). At certain frequencies (and thus, at certain times), the atom vapor will absorb some of the laser light, decreasing the amount of light that passes through the vapor. If this decrease in light, or absorption spectra, is observed, one can convert the time period of the laser scan into the frequencies the laser scanned over and apply that conversion to the absorption spectra, thereby determining the frequencies at which

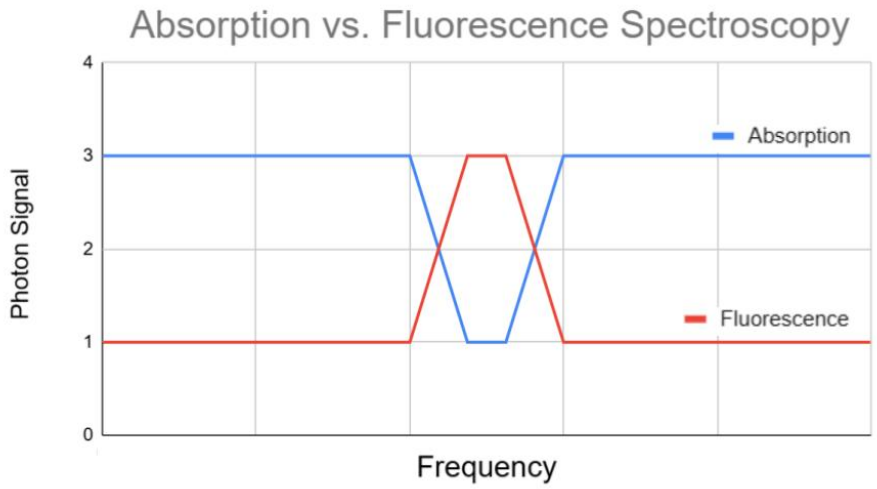

Figure 2.1: Diagram of absorption spectroscopy vs. fluorescence spectroscopy. Red graph signifies an absorption signal, while blue graph signifies a fluorescence signal. At resonant frequency, absorption spectroscopy shows a dip in photon signal while fluorescence spectroscopy shows photon emission.

energy transitions occur. Two spectroscopic methods specific to laser spectroscopy are Doppler broadened and laser saturated absorption spectroscopy.

Doppler broadened spectroscopy is named such because of the Doppler effect observed in the produced absorption spectra. The Doppler effect occurs when a source producing waves is moving relative to an observer. When approaching the observer, the frequency of the wave will appear to increase, and when traveling away from the observer, the frequency will appear to decrease (see Figure 2.2). Because atoms in a vapor naturally possess a variety of velocities from thermal motion, each atom in its own reference frame will observe incoming light as having a different relative velocity. Therefore, due to the Doppler effect, different atoms will also observe incoming light as having different frequencies. Only atoms with no velocity component in the same direction as the incoming light will observe it as having the at rest resonant transition frequency [7]. All other atoms in the vapor will observe light that is slightly

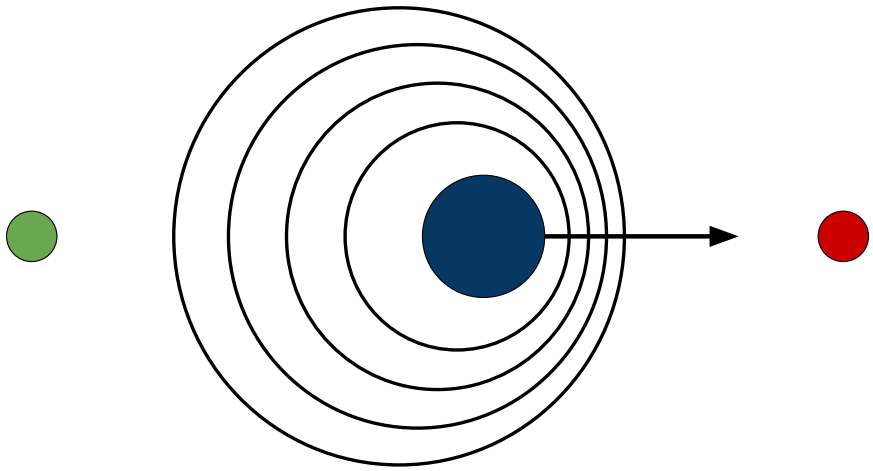

Figure 2.2: Diagram of the Doppler effect. Blue circle (center) generates wave while moving rightwards at constant velocity. Green circle (left) moves away with respect to blue circle, and observes wave with longer wavelength. Red circle (right) moves closer with respect to blue circle, and observes wave with shorter wavelength.

shifted away from the transition frequency, which causes Doppler broadening — the broadening of the absorption spectra lines of the vapor.

Doppler broadened laser absorption spectroscopy can be used to observe the regular and sometimes hyperfine structure of the energy levels of an atom (particularly for the ground states), but the broadening of the spectral lines is too significant to observe the hyperfine splittings of the excited energy levels. In order to observe the splittings, we can instead use laser saturated absorption spectroscopy. This method involves shooting two overlapping, counterpropagating lasers scanning at exactly the same frequency through a cloud of atoms. Because the lasers travel in opposite directions, the Doppler effect causes them to be resonant with two different groups of atoms while they scan - those with velocities in opposite directions. However, when the lasers are at the exact "at rest" resonant frequency of the atoms, they both interact with the same group of atoms - those with no component of velocity parallel to the

lasers. At this frequency, the stronger "pump" laser beam will reduce the amount of absorption that the weaker "probe" beam experiences by exciting many atoms out of the ground state. This results in dips in the Doppler broadened absorption spectrum around the resonant frequencies of the hyperfine structure energy levels [7].

In laser saturation spectroscopy, we can observe "crossover transitions" in addition to the transition lines of the hyperfine splitting energy levels. Crossover transitions occur when the pump and probe beams resonate with two different hyperfine transitions of non-zero velocity atoms at the same time. Due to the Doppler effect, the atoms moving with one velocity parallel to the beams will observe the lasers at one frequency, while the atoms moving with the opposite velocity component observes the lasers at a different frequency. At some frequency of the incoming lasers, both groups of atoms will observe the lasers at two different resonant frequencies at the same time, generating an extra transition line. Crossover transition lines occur halfway between hyperfine structure transition lines, and are often more prominent than the hyperfine structure transition lines. They occur when two transitions have the same ground state and have a smaller difference in frequency than the frequency amount of Doppler broadening [7]. Crossover transitions should not be confused with the spectral lines of the hyperfine structure transitions.

2.3 Electromagnetically-Induced Transparency

Electromagnetically induced transparency (EIT) is a slightly more complicated spectroscopic technique. The setup for this method is similar to that of laser saturation spectroscopy, where two counterpropagating lasers of different frequencies pass through and excite a vapor cloud of atoms, inducing a decrease in absorption at the exact resonant frequency. However, the physical process behind EIT is very different from saturation spectroscopy.

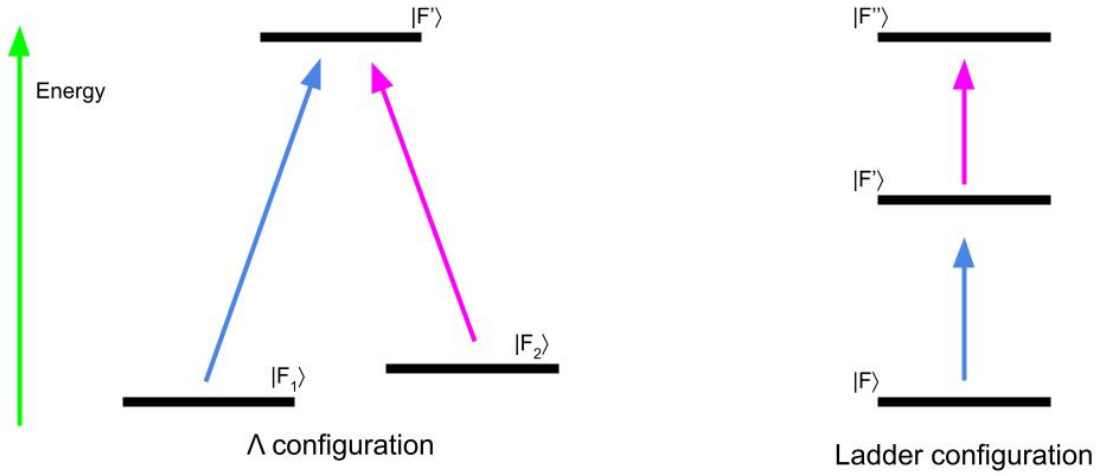

Figure 2.3: Diagram of electromagnetically induced transparency (EIT). Left displays Λ configurations (two ground states); right displays ladder configuration (one ground state). Figure adapted from [8].

Electromagnetically induced transparency can be performed in a Λ configuration or a ladder configuration (see Figure 2.3). In the Λ configuration, two lasers are used to excite two different ground states up to the same excited energy state. The energy (Hamiltonian) of this system can be found to have a "dark state," or a quantum superposition of both the ground energy states that effectively generates a destructive interference, and does not interact with either laser. Since atoms in the dark state do not interact with the lasers, they will not absorb the light, resulting in a transmission-induced dip in the atom's absorption spectrum. Thus, EIT is called such because the electromagnetic field of the second laser induces transparency or transmission around the resonant frequency. The ladder configuration is mathematically very similar to the Λ configuration; however, instead of the two lasers exciting from two ground states up to a common excited state, they excite from a ground state through a higher energy state up to an extremely excited state [8].

Chapter 3

Methods

3.1 Basics of Spectroscopy

In this section, I will elaborate on the tests I conducted to measure the 5S and 5P levels of rubidium. In order to reach the 5D levels of rubidium, one must excite from the 5S levels through the 5P levels; knowledge of these levels is integral in efficiently exciting to the 5D levels. Additionally, in measuring these levels, I took the opportunity to learn and practice different spectroscopic techniques, so I could ultimately utilize my knowledge and experience to measure rubidium's 5D levels.

3.1.1 5S Levels: Fluorescence & Doppler Broadened Absorption Spectroscopy

Performing fluorescence spectroscopy and Doppler broadened absorption spectroscopy in an vapor cell of rubidium atoms allowed for the measurement of the $5S_{1/2}$ hyperfine structure levels of rubidium. For this process, one laser scanning at 780 nm was beamed through the vapor cell and into a photodetector (see Figure 3.1). The photodetector connected to an oscilloscope so that the photons detected could be graphed and read as voltages. Additionally, a video camera was placed near the vapor cell to observe fluorescence in the rubidium cell when the laser was correctly aligned and on resonance (see Figure 3.2).

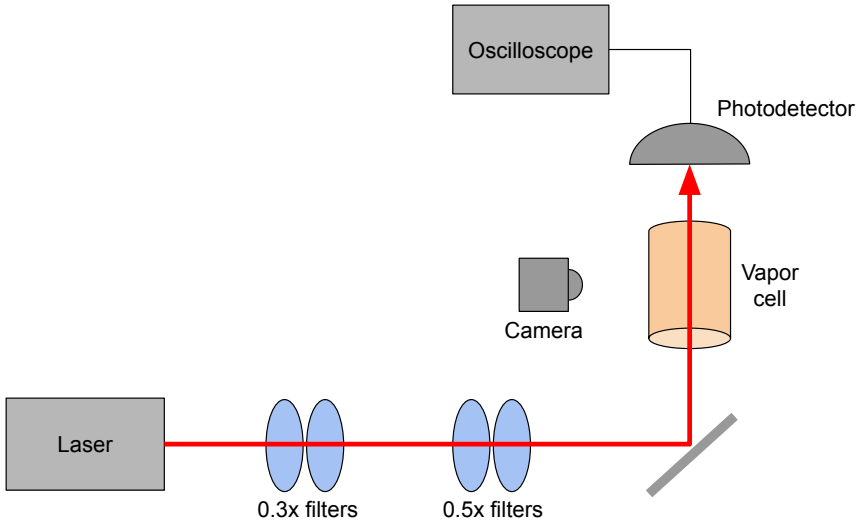

Figure 3.1: Diagram of experimental setup for Doppler broadened spectroscopy in a vapor cell. Laser is set to scan at 780 nm.

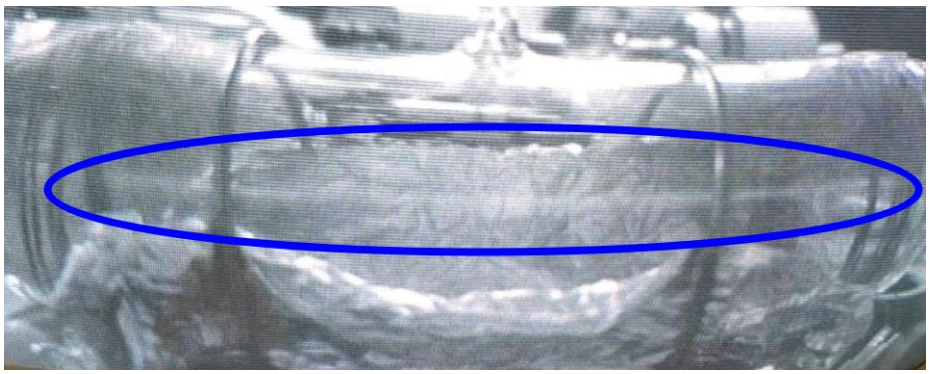

Figure 3.2: Camera image of fluorescence in rubidium vapor upon de-exciting from the 5P to 5S levels at the resonant frequency of excitation. Blue circle encloses line of fluorescence.

The resulting graph displayed four absorption spectrum peaks, which is the expected result for rubidium (see Figure 3.3). This is because the natural rubidium in the vapor cell consists of both of rubidium's natural isotopes (^{87}Rb and ^{85}Rb), and each isotope has two distinct hyperfine structure levels within the $5S_{1/2}$ energy level (F=1,2 for ^{87}Rb, and F=2,3 for ^{85}Rb) [9] [10]. Thus, four peaks are to be expected —

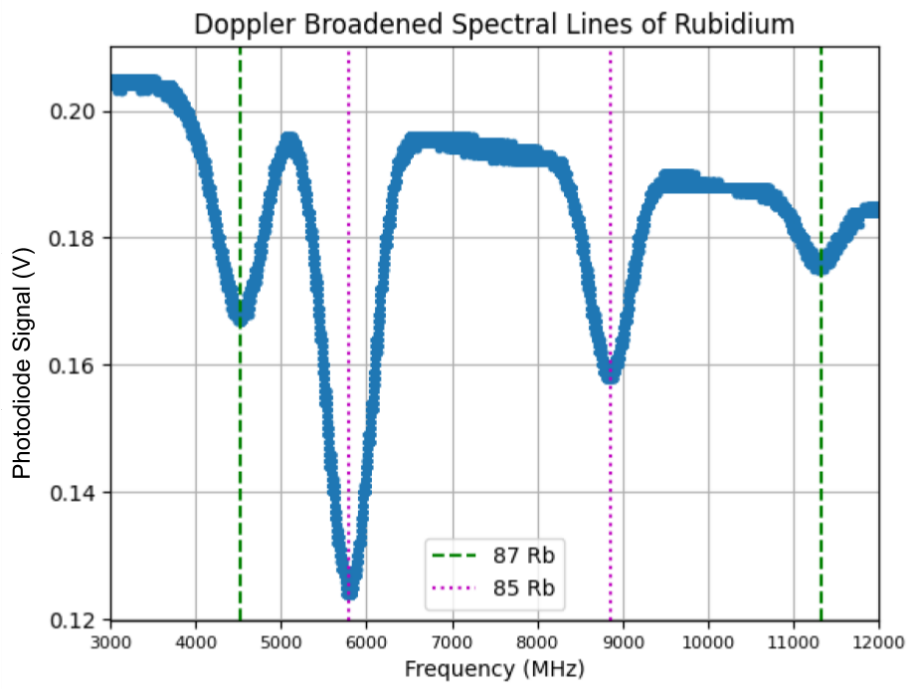

Figure 3.3: Frequency vs. photodiode signal graph of Doppler broadened spectral lines of $5S_{1/2}$ hyperfine levels for ^{87}Rb (outer peaks, labeled in green) and ^{85}Rb (inner peaks, labeled in pink).

two for each isotope. Because ^{85}Rb is the more common isotope in natural rubidium, its absorption lines were stronger than the ones for ^{87}Rb, as more ^{85}Rb atoms means more light will be absorbed at their resonant frequency.

These four peaks are the result of the rubidium's excitation from the 5S levels to the $5P_{3/2}$ levels. However, because of the Doppler broadening, we cannot make out the hyperfine structure transition peaks for the $5P_{3/2}$ levels. Instead, we can determine the separation between the $5S_{1/2}$ hyperfine structure levels, as both of the hyperfine structure energy levels for each rubidium isotope will excite to the $5P_{3/2}$ level at different frequencies. Thus, the separation between the $5S_{1/2}$ hyperfine levels is the separation between the Doppler broadened absorption spectrum peaks.

The purpose of this process was to measure the transition frequencies between the

$5S_{1/2}$ hyperfine structure energy levels. After visually analyzing the data to determine the locations of the peaks and using the known values of the transition separations to convert the original time scaled x-axis of the oscilloscope data to a frequency scale, the $5S_{1/2}$ separation was measured as follows, with the percent difference from the known values (also shown below) of 0.5%:

Observed $5S_{1/2}$ Hyperfine Splittings (MHz)		Accepted Values (MHz)
^{85}Rb	3051.7 ± 99.6 MHz	3035.7 MHz
^{87}Rb	6799.0 ± 120.7 MHz	6834.7 MHz

Time to Frequency Conversion Factor
2838.8 ± 14.9 MHz to 1 second

Table 3.1: Observed and accepted values for hyperfine splittings of the $5S_{1/2}$ levels of ^{85}Rb and ^{87}Rb, found using Doppler broadened spectroscopy. Accepted/known values from [9] and [10]. Laser scan conversion factor from time to frequency is also included.

3.1.2 5P Levels: Laser Saturated Absorption Spectroscopy & Ground State EIT

In order to find the hyperfine structure of the $5P_{3/2}$ level of rubidium, laser saturated absorption spectroscopy was performed on a vapor cell of rubidium atoms. This method only required the use of one laser at 780 nm; however, a beam splitter was used to separate it into three separate beams. Two probe beams, which were observed with photodetectors, passed through the vapor cell from one direction, and a counterpropagating pump beam, which induced saturation, passed through the cell from the opposite direction. The pump beam interacted with one of the probe beams; the other probe beam was a control beam for reference (see Figure 3.4).

Two separate signals from individual photodetectors are obtained through this setup. One signal is the same Doppler broadened absorption spectrum discussed above, while the second possesses the dips characteristic of laser saturated absorption

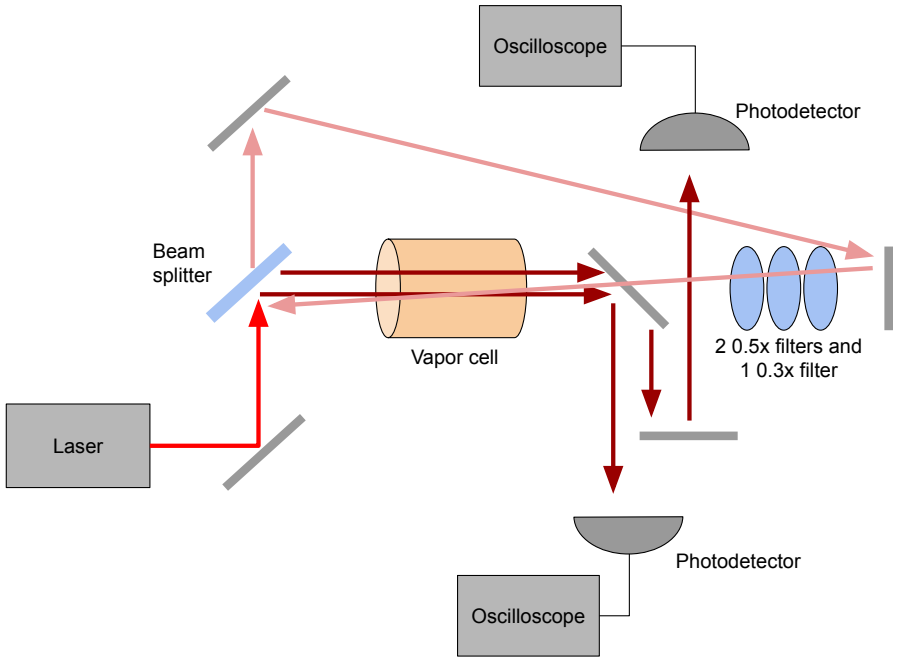

Figure 3.4: Diagram of experimental setup for laser saturated absorption spectroscopy in a vapor cell. Light red arrows are the pump beam, dark red arrows are the probe beams.

spectroscopy (see Figure 3.5). In order to observe only the transition peaks, the two signals are subtracted from each other so that only the difference (the peaks) remains.

Though hypothetically, one could observe the hyperfine splitting transitions within either of the larger Doppler broadened transition peaks for both rubidium isotopes, the two peaks that were selected to analyze were those with the clearest saturation spectroscopy dips. Ultimately, the most suitable peaks were the most prominent peaks for ^{87}Rb and ^{85}Rb. Each isotope displayed six dips/peaks, which is expected for the $5P_{3/2}$ states of rubidium [9] [10] — three of these peaks are transition peaks and three are crossover peaks, which are halfway between the transition peaks (see Figures 3.6 and 3.7).

In order to obtain the peak separations, the data was fit to the sum of six

Figure 3.5: Oscilloscope frequency vs. potential data of Doppler broadened absorption lines of rubidium with and without 5P saturation spectroscopy dips. Above (pink) graph displays data with laser saturated absorption spectroscopy features, below (yellow) graph displays data without.

Lorentzian functions (see Equation 3.1), estimating the amplitude A, width d, and position x_o of each peak to use as initial parameters for the fits.

$$y = \frac{Ad^2}{d^2 + (x - x_o)^2} \tag{3.1}$$

For ^{85}Rb, not all six peaks were clearly defined, so the fact that crossover transition peaks are exactly halfway between each pair of transition peaks was used to estimate the position of the sixth "invisible" peak.

After fitting the data of ^{85}Rb and ^{87}Rb, the original time-scaled x-axis of the oscilloscope data must be converted to a frequency scale. This was done by taking the ratios of the time difference of both hyperfine splittings for an isotope to the known frequency values of the splittings, then averaging the two ratios to obtain a conversion factor. After this conversion, the separation between the hyperfine structure transitions could be measured. The measured hyperfine splittings of the $5P_{3/2}$

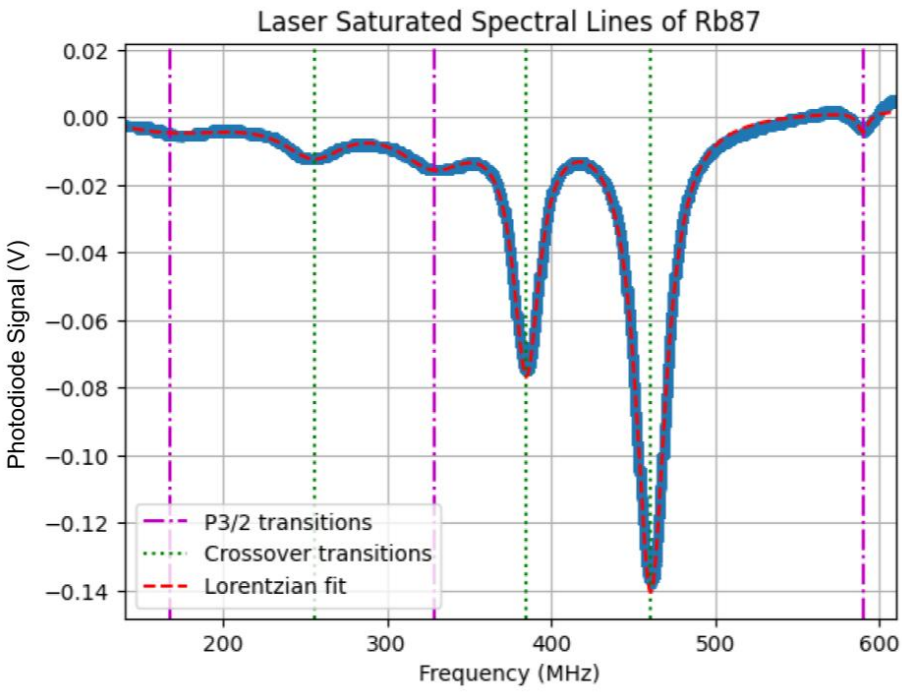

Figure 3.6: Frequency vs. potential graph of laser saturated spectral lines and crossover transition lines of $5P_{3/2}$ level of ^{87}Rb, fit with a sum of six Lorentzian functions (Equation 3.1).

levels for rubidium-87 can be seen in Figure 3.6 and Table 3.2, and have a percent difference from the known values of 2.2%. The measured splittings for the same level in rubidium-85 can be seen in Figure 3.7 and Table 3.3, and have a percent difference from the known values of 8.5%.

^{87}Rb Observed $5P_{3/2}$ Hyperfine Splittings (MHz)		Accepted Values (MHz)
F=1 → F=2	160.8 MHz ± 8.1 MHz	156.9 MHz
F=2 → F=3	261.4 MHz ± 14.8 MHz	266.7 MHz

Time to Frequency Conversion Factor
10849.4 ± 237.5 MHz to 1 second

Table 3.2: Observed and accepted values for hyperfine splittings of the $5P_{3/2}$ levels of ^{87}Rb, found using laser saturated absorption spectroscopy. Accepted/known values from [10]. Laser scan conversion factor from time to frequency is also included.

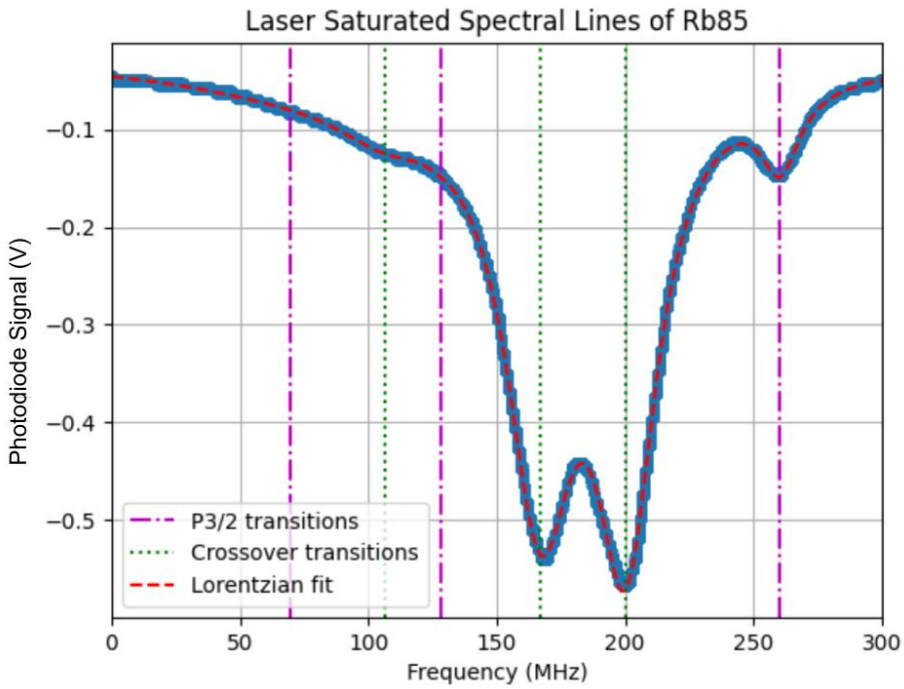

Figure 3.7: Frequency vs. potential graph of laser saturated spectral lines and crossover transition lines of $5P_{3/2}$ level of ^{85}Rb, fit with a sum of six Lorentzian functions (Equation 3.1).

^{85}Rb Observed $5P_{3/2}$ Hyperfine Splittings (MHz)		Accepted Values (MHz)
F=2 → F=3	58.3 MHz ± 12.7 MHz	63.4 MHz
F=3 → F=4	132.2 MHz ± 25.2 MHz	120.6 MHz

Time to Frequency Conversion Factor
11351.6 ± 983.9 MHz to 1 second

Table 3.3: Observed and accepted values for hyperfine splittings of the $5P_{3/2}$ levels of ^{85}Rb, found using laser saturated absorption spectroscopy. Accepted/known values from [9]. Laser scan conversion factor from time to frequency is also included.

To test the setup for observing electromagnetically-induced transparency of the 5D levels, a test of ground state (Λ) EIT was performed on the $5P_{3/2}$ levels and features resembling EIT were observed. The setup for this method involved two counterpropagating lasers at 780 nm. One laser was locked at the resonant frequency,

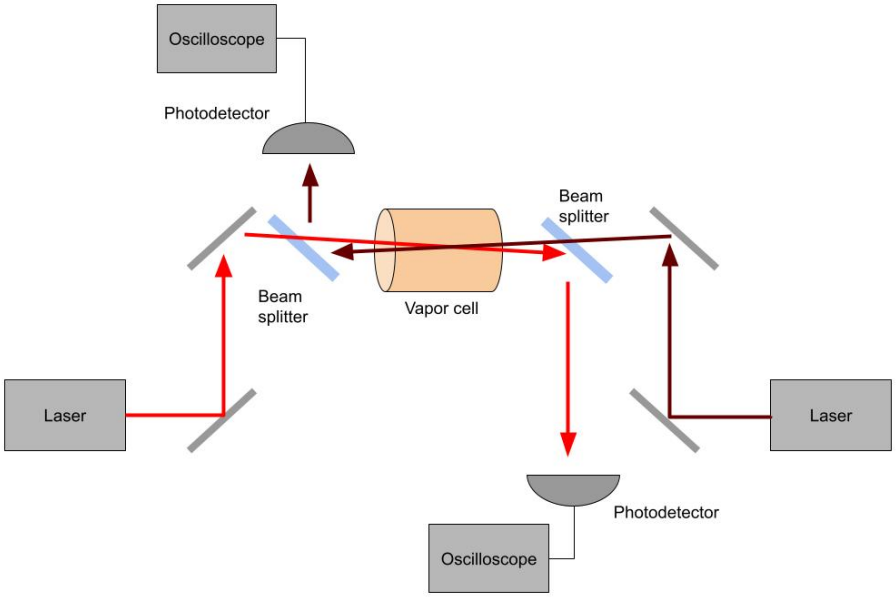

Figure 3.8: Diagram of experimental setup for ground state EIT in a vapor cell. Bright red arrow is locked laser, dark red arrow is scanning laser.

while the other was scanning around it. Photodetectors were used to observed the scanning and locked lasers (see Figure 3.8).

Structure resembling EIT was observed on both the scanning and locked laser. On the scanning laser, the structure was observed on the ^{87}Rb peaks, which is expected because the locked laser was locked on a ^{87}Rb peak. Increased absorption was observed on the smaller peak, which is surprising (see Figure 3.9), but the larger peak displays a decrease in absorption, which was as expected (see Figure 3.10). With repeated observations on different days, the structure observed occurred at different points in the Doppler broadened absorption peak, but was always spaced apart by approximately the same frequency. This could be due to the laser's frequency drifting over time.

Because this segment was a test of the experimental setup, the structure has not currently been analyzed further. The experimental setup successfully observed fea-

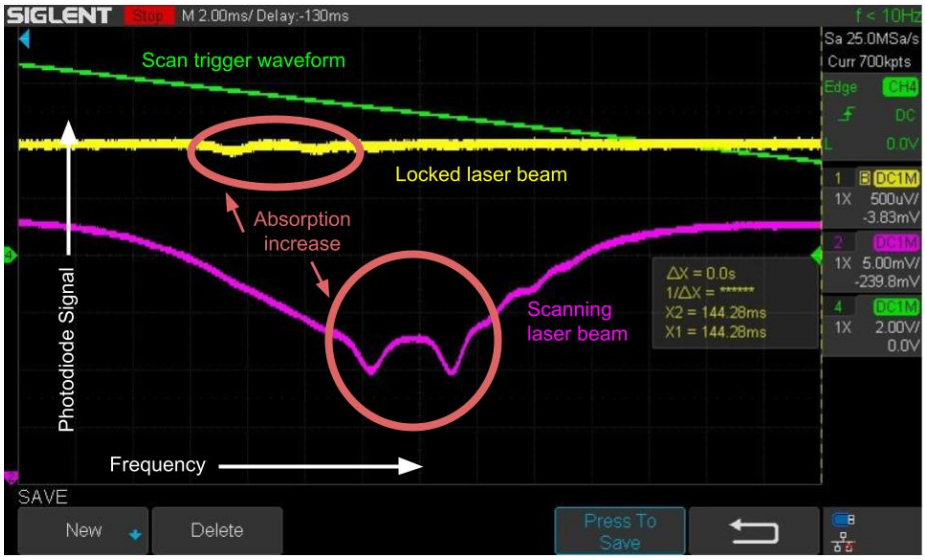

Figure 3.9: Oscilloscope photodiode signal vs. frequency data of ground state EIT-like features for one peak of the 5S levels of ^{87}Rb, featuring increased absorption. Above (yellow) graph displays data from locked laser; below (pink) graph displays data from scanning laser. Green graph is oscilloscope trigger waveform.

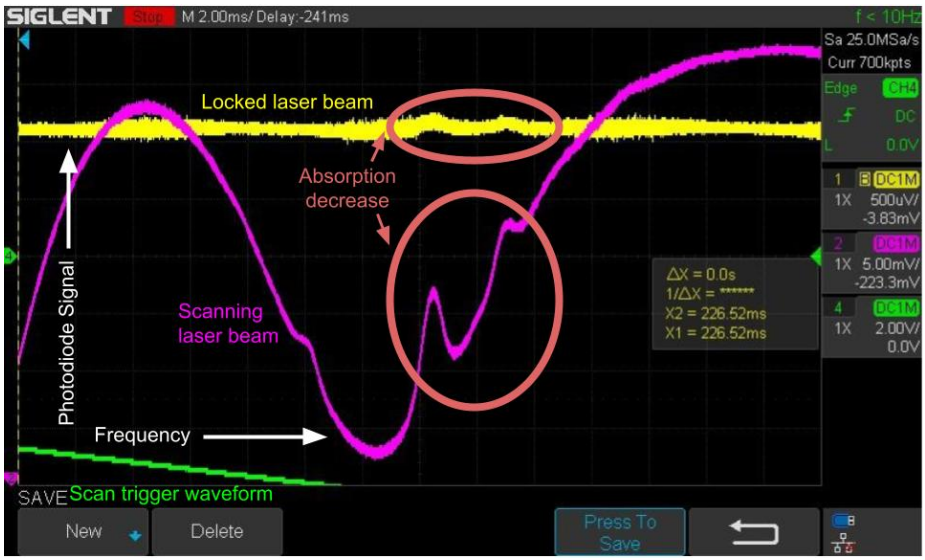

Figure 3.10: Oscilloscope photodiode signal vs. frequency data of ground state EIT-like features for one peak of the 5S levels of ^{87}Rb, featuring decreased absorption. Above (yellow) graph displays data from locked laser; below (pink) graph displays data from scanning laser. Green graph is oscilloscope trigger waveform.

tures resembling ground state EIT, so it would most likely be successful in observing EIT on the 5D levels in future research.

3.2 Measuring the 5D Levels

In this section, I discuss the methods by which I measured the 5D energy levels of rubidium. This mainly involves fluorescence spectroscopy in a vapor cell, but also includes fluorescence detected in a cold atom apparatus.

3.2.1 5D Fluorescence Spectroscopy in Vapor Cell

Fluorescence spectroscopy was one method used to observe the 5D energy levels of rubidium. This method involved using two lasers of different wavelengths to excite the rubidium atoms through the 5P and up to the 5D energy levels, similarly to how a laser is used to excite the rubidium atoms to the $5P_{3/2}$ level in the previous section. After being excited to the 5D levels, which are unstable, the rubidium atoms would lose energy and de-excite through the 6P levels (see Figure 1.1). When de-exciting from the 6P levels to the ground state, the wavelength of light emitted is approximately 420 nm, which corresponds to blue visible light. Fluorescence spectroscopy was used to determine when the scanning laser's frequency was resonant with the 5D rubidium levels, as the rubidium emitted blue photons at this frequency.

In order to excite rubidium to the 5D levels, two lasers were necessary - one at 780 nm and one at 776 nm. The precise excitation value for the 780 nm laser was known from the first part of this experiment; the specific transition wavelength of the 776 nm laser still had to be determined so as to not endure a lengthy search for the transitions. I could not find a specific enough value for the 776 nm transition could not be found when looking through other sources; however, I did find the precise wavelength value for a different method of exciting rubidium to the 5D levels — by

using two 778 nm lasers. Both the 780/776 nm method and the 778/778 nm method excite rubidium to the $5D_{5/2}$ levels, and one set of wavelengths can be used to find the other. Although one cannot add and subtract wavelengths to determine the values of different transitions, it is possible to convert a wavelength to an energy (in units of inverse centimeters) and add and subtract energies together.

According to the International Bureau of Weights and Measures, rubidium can be excited to the 5D levels using two lasers of 778.105 nm in a vacuum [11]. This value can be converted to inverse centimeters using the following formula:

$$1cm^{-1} = \frac{1}{1nm} \times 10^7 \tag{3.2}$$

778.105 nm becomes 12851.7 cm^{-1}. We know from the first part of this experiment that the exact value for the 780 nm transition is 780.250 nm in a vacuum (or 12816.4 cm^{-1}). One can then set the sum of the inverse centimeter values for one method of excitation to the sum of the values for the other method.

$$2 \times 12851.7 = 12816.4 + x \tag{3.3}$$

Through this method, the value for the 776 nm transition was found to be x=12887.1 cm^{-1} or 775.971 nm.

The setup to excite rubidium in a vapor cell to the 5D levels involved two counterpropagating lasers aligned with each other passing through the vapor cell. One laser was locked at 780 nm, and the other laser was scanned centered at 775.971 nm (initially). In order to observe fluorescence spectroscopy, a photomultiplier tube (PMT) was necessary, as it could detect the emitted photons from the vapor cell and connected to a photon counter and oscilloscope so that the data could be collected (see Figure 3.11). The detector end of the PMT needed to be as close as possible to the vapor cell in order to see the fluorescence, and the opposite end needed to have access to the cables and ports so that it could be powered and the data could be read.

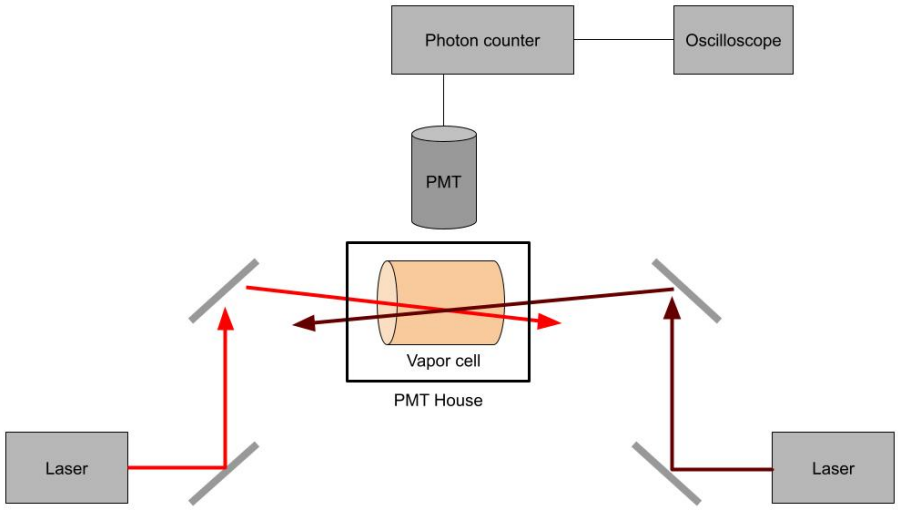

Figure 3.11: Diagram of experimental setup for fluorescence spectroscopy in a vapor cell. Bright red arrow is locked 780 nm laser, dark red arrow is scanning 776 nm laser. The photomultiplier tube is held above the vapor cell using a stand.

A stand for the PMT was built so that it could be suspended above the vapor cell, while still granting access to the cable ports (see Figure 3.12).

A 420 nm filter was placed over the entrance to the PMT, blocking most ambient light in the room and only allowing in light at the emission wavelength when rubidium decays from the 5D levels. However, even with the filter, there still was too much ambient light entering the PMT for it to easily detect fluorescence. A "house" for the PMT was constructed to block ambient lighting. The PMT house was made of black cardboard and held together with black electrical tape. The dark colors absorbed light instead of reflecting it off and into the PMT. The vapor cell sat inside the PMT house, as did the detector end of the PMT. The house consisted of four walls, with holes in two of them to allow the laser to pass through and enter the vapor cell inside. Initially, there was no roof on the PMT house. Before constructing the PMT house, the photon counter detected a photon frequency of greater than 100 photons from the room's ambient lighting. After constructing the PMT house, the

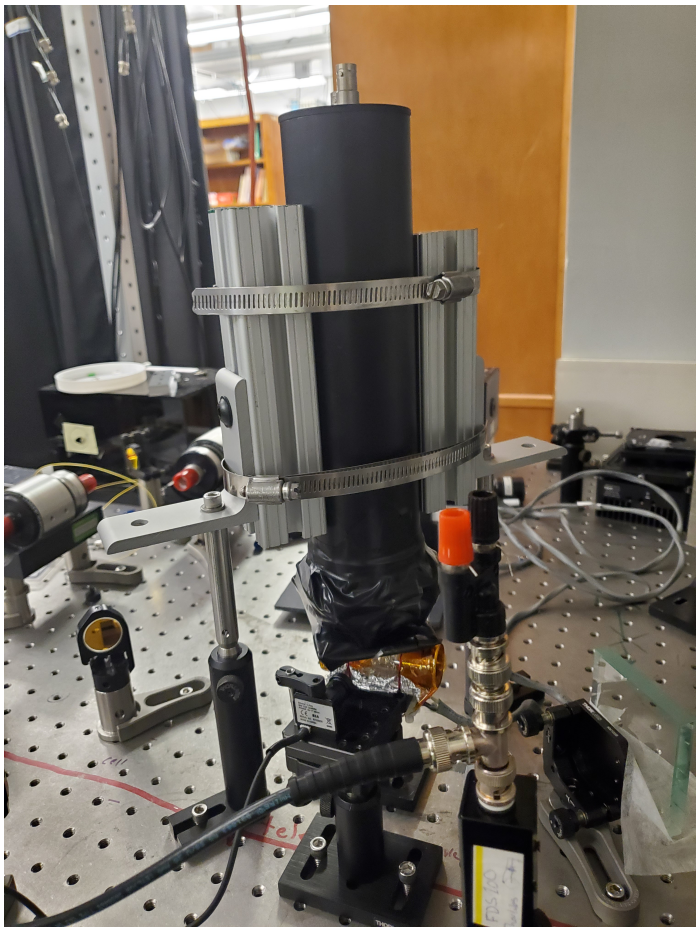

Figure 3.12: Constructed PMT stand, holding photomultiplier tube above rubidium vapor cell. Later, PMT "house" is placed around vapor cell.

photon counter detected a photon frequency of less than 10 photons. The PMT house greatly decreased the amount of noise from ambient lighting that the PMT detected.

Fluorescence could then be observed. Using a wavemeter, the scanning laser was set to scan around approximately 775.971 nm. The 780 nm laser was locked to the $5D_{3/2}$ transition with a power of 0.14 mW entering the vapor cell, and the 776 nm laser scanned with a power of 0.93 mW entering the cell. The scanning laser's wavelength was changed very slightly until two spikes appeared from the PMT signal on the connected oscilloscope. Upon decreasing the scanning amplitude of the laser to "zoom in" on the spiking signal, these spikes could be confirmed to be the

result of fluorescence of the rubidium atoms (and not just noise), as when one of the lasers exciting the rubidium atoms was blocked, the spikes/peaks disappeared. The photopeaks were measured to occur at a wavelength of 775.9776 nm using a wavementer.

After the initial construction and testing of the fluorescence spectroscopy setup, my experiment was moved to a different room (from Professor Seth Aubin's lab to Professor Irina Novikova's) to account for availability of space and lasers. Thus, the setup and results were replicated, with slight changes. The PMT house was rebuilt, with the addition of a "roof" to block ambient light from above. The second version of the PMT house also decreased the photon counter to a photon detection frequency of less than 10 photons per second.

Additionally, in the second iteration of the fluorescence spectroscopy setup, the height of the laser and optics equipment was standardized to 2 inches (the standard for Professor Novikova's labs). A pedestal for the 776 nm laser had to be created to achieve this standardized height. The laser pedestal was made of aluminum and had dimensions of 5x10x2 inches, with a 7/8 inch tall and 1/2 inch deep groove carved into the sides to attach the pedestal to the table and four 1/4"-20 threaded holes to attach the laser to the pedestal (see Figure 3.13). It was made primarily using the miller machine and a hand tapping tool.

Because the 776 and 780 nm lasers for my setup now needed to be shared with fellow student Kevin Su, the setup also changed slightly. A 50/50 beam splitter cube was placed in front of the 776 nm laser, so half of the laser's power was sent to my experiment while the other half was sent to Su's. Additionally, a rotating half wave plate and a polarizing beam splitter cube were placed in front of the 780 nm laser, so that when the half wave plate was turned it could send the laser's power to Su's experiment or mine, depending on who needed it at the moment. Two photodetectors

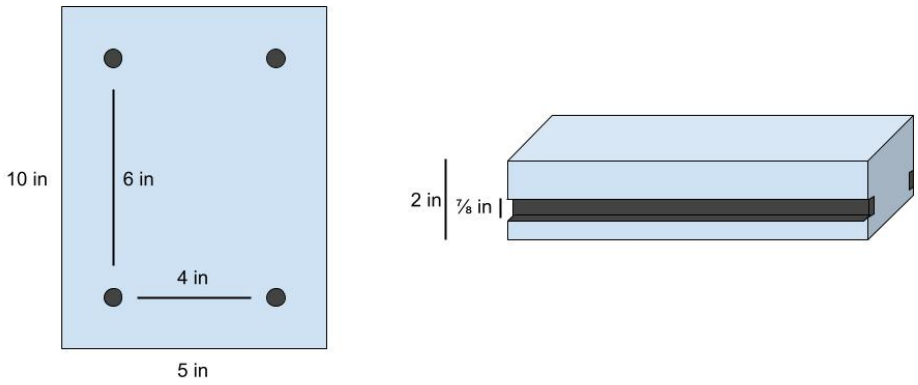

Figure 3.13: Diagram of the aluminum pedestal made to hold the 776 nm laser.

were also added to the setup, each detecting the light from a laser after it passed through the vapor cell. This was initially done with the intent of using them to detect EIT in the vapor cell, but as that goal was not realized, the photodetectors were mainly used to ensure that the laser beams remained aligned in the cell. Figure 3.14 depicts the improved version of the fluorescence spectroscopy setup.

In addition to sharing the 780 nm laser with Su, it also needed to be shared with Dr. Mykhailo Vorobiov, a postdoctoral researcher in the same lab. To do this, we utilized a 1x2 fiber coupler, where one output went to Vorobiov's experiment and the other went to Su's and I's. The coupler's power output was tested and compared to its input due to fears of insufficient power, and it was determined that the coupler output was approximately 50% of input power from each output terminal - the expected amount.

In my efforts to observe EIT, it was determined that the vapor cell would likely need to be heated to increase the observed photon signal, as the heat would increase the density of the rubidium atoms. There was a heating mechanism attached to the vapor cell, comprised of several wires wrapped around each end (so that when heated, the rubidium did not condense on the otherwise cooler faces of the cylindrical vapor

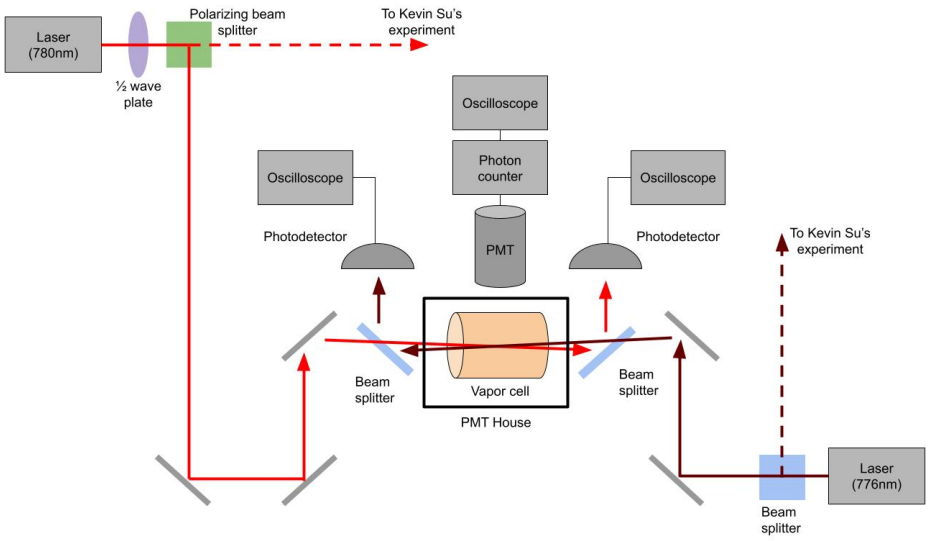

Figure 3.14: Diagram of experimental setup for 5D fluorescence spectroscopy in a vapor cell. Bright red arrow is locked 780 nm laser, dark red arrow is scanning 776 nm laser. PMT is held above vapor cell using stand.

cell) that could be plugged into a power source. However, during the first iteration of this experiment, the wires had become disconnected and did not heat. Instead, a heat gun was used to briefly heat the vapor cell. When the experimental setup was replicated in the other room, the wires were fixed and could be used to heat the vapor cell much more efficiently with an applied power of 3 Watts at a current of 1.2 Amps (2.5 Volts). Though EIT was ultimately not observed for the 5D levels, fixing the vapor cell's heating mechanism will assist in its potential observation in the future.

During winter break, PhD student William Miyahira discovered that when the lasers hit the vapor cell head-on, it caused reflections within the cell that generated extra peaks and irregular structure. However, when the cell was rotated to be in diagonal with the laser beams, the reflections disappeared and resulted in a much clearer spectrum. Thus, in the replicated setup, the vapor cell was slowly rotated until the reflection spectra disappeared.

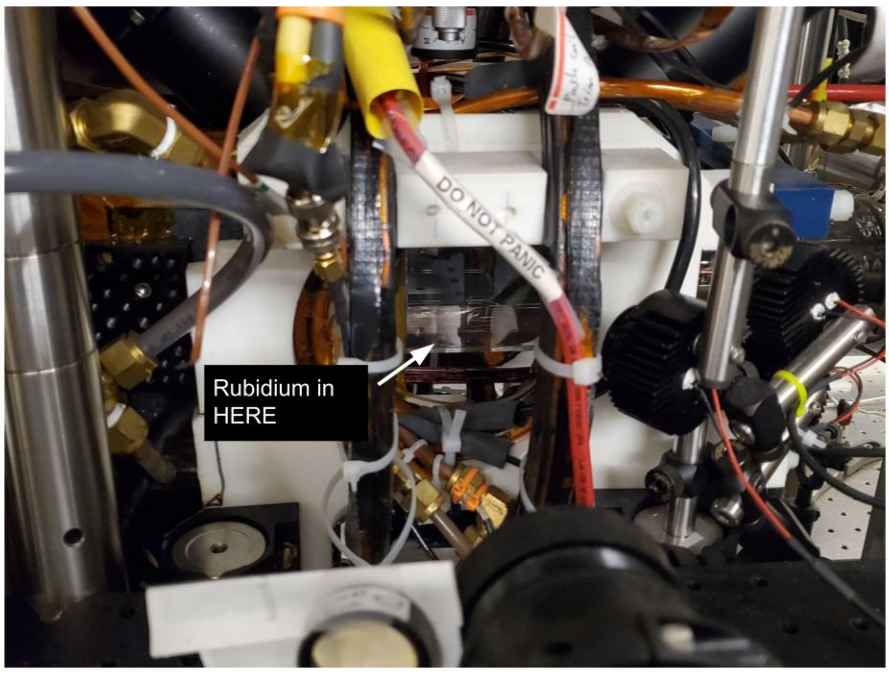

Figure 3.15: Photograph of the magneto-optical trap (MOT) in the cold atom apparatus.

3.2.2 5D Fluorescence in the Cold Atom Apparatus

After finding the resonant frequencies of rubidium in a vapor cell, these laser frequencies were used in the cold atom apparatus (Figure 3.15) to induce fluorescence. The exact process and setup for this part of the experiment was completed during winter break by William Miyahira, and was finalized during the first week of the spring semester.

This process involved shooting both the locked 780 nm laser and scanning 776 nm laser into the cold atom apparatus to interact with the atoms in the ^{87}Rb magneto-optical trap (MOT). Much like in a vapor cell, the atoms in the MOT would fluoresce blue upon absorbing the resonant frequency from the 776 nm laser. The data from this process was recorded by both ordinary cameras and by camera data analysis software that is used to analyze data in the MOT.

Chapter 4

Results and Analysis

This chapter details the results of measuring the 5D transition levels and hyperfine splittings of the 5D levels of rubidium using fluorescence spectroscopy. The first section of this chapter examines measurements in a vapor cell, while the second section uses a cold atom apparatus.

4.1 5D Fluorescence in Vapor Cell

During the first iteration of the experiment, fluorescence was observed at the $5D_{5/2}$ levels of rubidium-87 by scanning the 776 nm laser around a 775.9776 nm wavelength (see Table 1.1). Fluorescence was initially detected as a singular photopeak over the laser's scanning period, seen as two peaks as the laser scans up and down through the same frequency (see Figure 4.1). Notably, the photopeaks were not symmetric relative to the laser's scanning frequency - they appeared to occur at different frequencies when the frequency increased compared to when it decreased. This was likely due to hysteresis effects in the laser's piezo, where the frequency of a laser changed depending on whether the scanning voltage was increasing or decreasing. Upon discovery of the photopeak at the resonant wavelength, the scanning frequency range was slowly decreased until the fluorescence peaks could be resolved more finely. At finer resolution, three peaks were detected at the $5D_{5/2}$ level (see Figure 4.2) — a

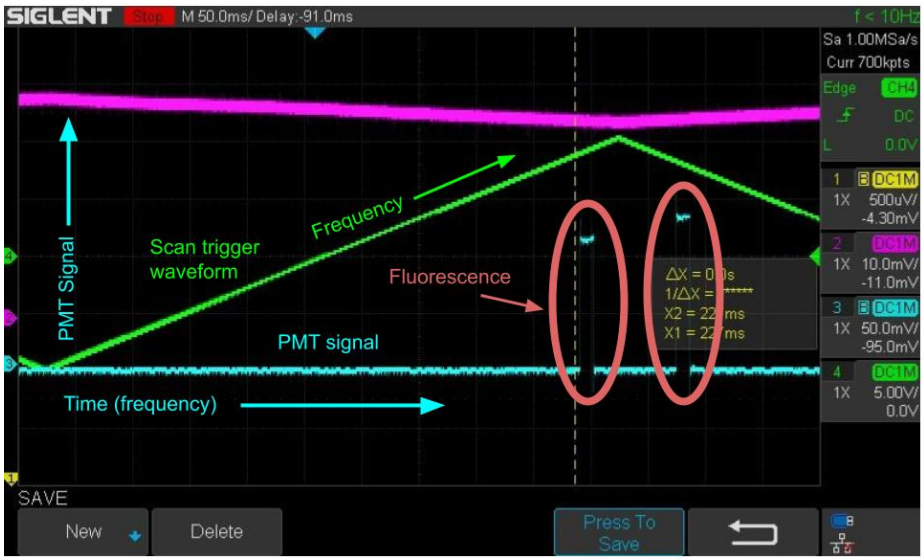

Figure 4.1: Oscilloscope PMT signal vs. time (frequency) data of fluorescence spectroscopy for $5D_{5/2}$ level of rubidium-87. Blue graph displays PMT data. Two photopeaks can be seen; these are the same peak, visible twice because the 776 nm laser scans back over the same frequency (displayed by the green graph).

large peak, a small peak, and an even smaller peak.

5D Transition	Resonant Frequency (nm)
$5D_{5/2}$	775.9776 ± 0.0001 nm

Table 1.1: Resonant wavelengths for 5P to 5D transitions of rubidium in nanometers, determined by fluorescence spectroscopy. Error is statistical.

Initially, the structure of the large peak changed over time. However, upon multiple repetitions of this iteration of the experiment over multiple days, whether the peak structure would change or stay the same over time varied. During winter break, graduate student William Miyahira discovered that some of the initially observed variation and structure of the photopeaks was caused by reflections of the laser inside the vapor cell. Because the laser entered and exited the vapor cell head-on, it would reflect off the faces of the cell back into itself. The interaction between the original and reflected beams would cause extra peaks and variation in structure to

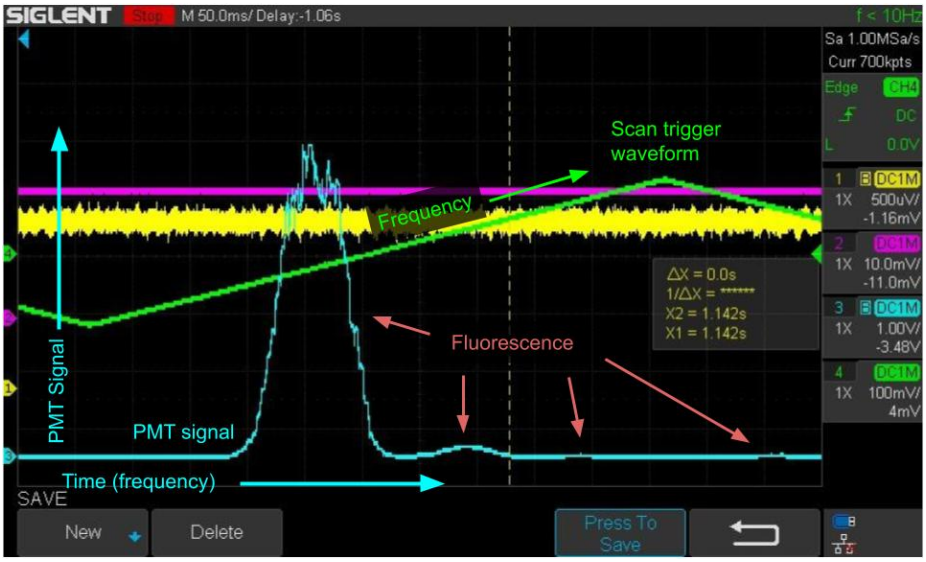

Figure 4.2: Oscilloscope PMT signal vs. time (frequency) data of fluorescence spectroscopy for $5D_{5/2}$ levels of rubidium-87 from first iteration of experiment. Blue graph displays PMT data. Three photopeaks can be seen: the largest on the left, a smaller peak to the right, and an even smaller peak further right. The smallest peak is mirrored around the peak of the green (trigger) graph, which is expected as the frequency oscillates.

Figure 4.3: Diagram of rotation of vapor cell, with respect to incoming laser

form. This issue was eliminated by rotating the vapor cell, so that the laser did not reflect directly into itself upon entering and exiting the cell (see Figure 4.3). When the cell was rotated, the extra photopeaks and structural variation that was initially observed disappeared.

The second iteration of this experiment observed the $5D_{5/2}$ levels of both rubidium-85 and rubidium-87. Additionally, in the second iteration of this experiment, the

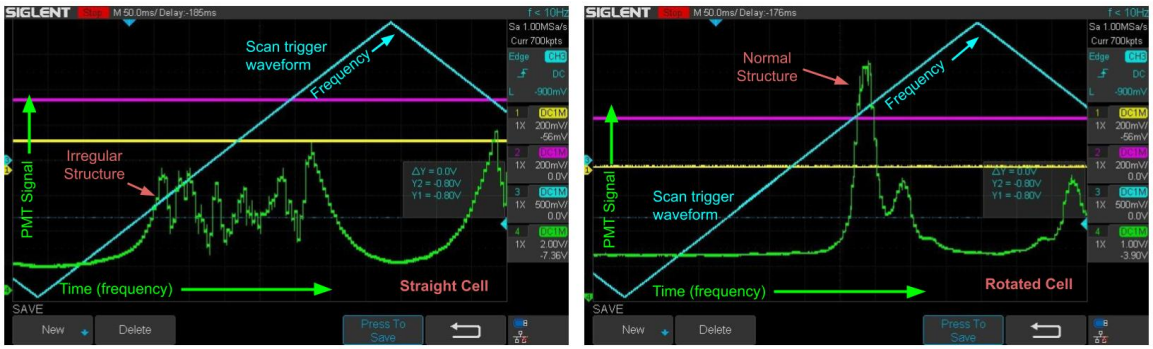

Figure 4.4: Oscilloscope PMT signal vs. time (frequency) data of $5D_{5/2}$ fluorescence spectroscopy of rubidium-85 in a vapor cell. Left side displays data when vapor cell is not rotated, observing extremely irregular photopeak structure. Right side displays data when vapor cell is rotated, observing only three photopeaks.

need to rotate the vapor cell was considered. The impact of the vapor cell's rotation on the structure of the photopeaks can be seen in Figure 4.4; the structure of the photopeaks changed from very irregular before the cell was rotated to a much more normal Lorentzian shape after rotation.

Calibration of the x-axis was needed to determine the splittings between the hyperfine levels. Firstly, the conversion from piezo control voltage to wavelength needed to be determined. This was done by slowly changing the piezo voltage control to the 776 nm laser (from -10 to +10 volts, in one volt intervals) and measuring the corresponding wavelength using a wavemeter. Wavemeter data from each measured piezo voltage was averaged, then the averaged wavelengths were plotted against the corresponding piezo voltage and fit with the following cubic function (see Figure 4.5), where x is piezo voltage in volts and y is wavelength in nanometers:

$$\begin{aligned} y = (8.469 \times 10^{-8} \pm 0.03548)x^3 - (1.605 \times 10^{-6} \pm 0.1970)x^2 - \\ (1.542 \times 10^{-4} \pm 2.514)x + (775.976452 \pm 9.4474670) \end{aligned} \tag{4.1}$$

After converting the piezo control voltage into wavelength, the time period of the laser's scan then had to be converted to into a wavelength scale. Since the laser

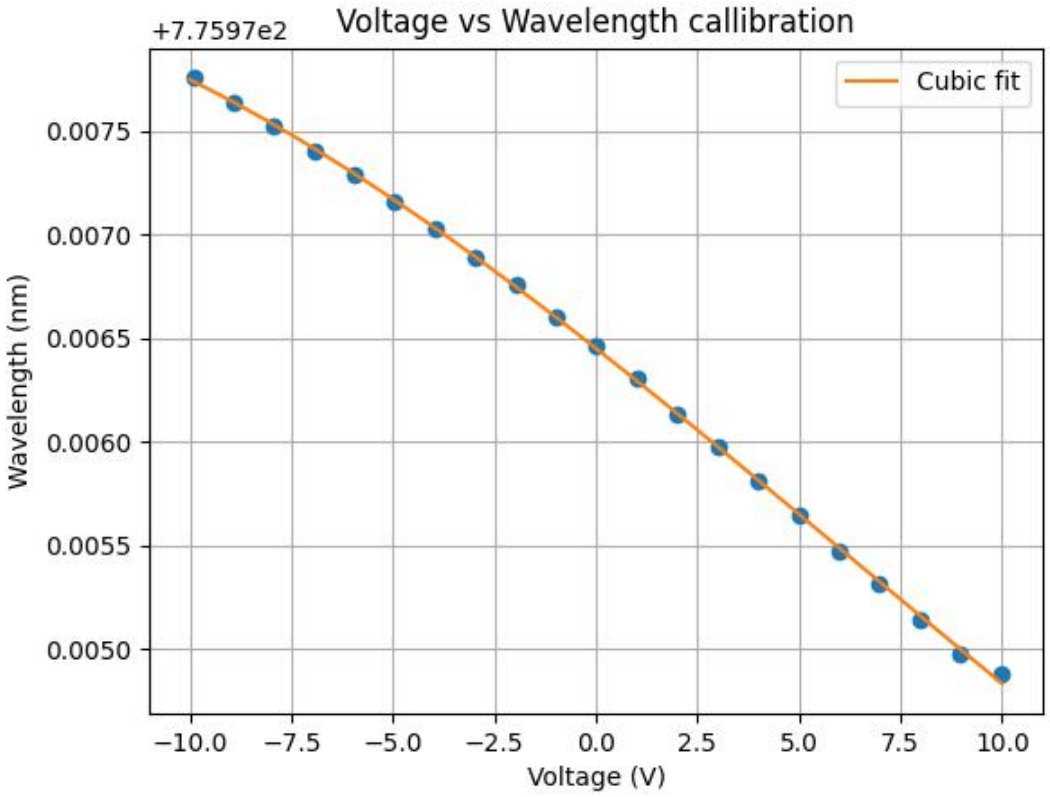

Figure 4.5: Cubic best fit for calibration conversion from laser piezo control voltage to laser best fit wavelength. Cubic fit equation is Equation 4.1.

scanned as a triangle wave over time, this was done with a simple linear fit where x is time in seconds and y is wavelength in nanometers:

$$y = -0.001209x + 775.9764144 \tag{4.2}$$

After this, the only necessary conversion remaining was one of convenience: converting wavelength into frequency, using the simple equation

$$\lambda = \frac{c}{\nu} \tag{4.3}$$

where λ is wavelength, ν is frequency, and c is the speed of light. The fluorescence spectroscopy data was could then be plotted as a function of PMT signal vs. frequency

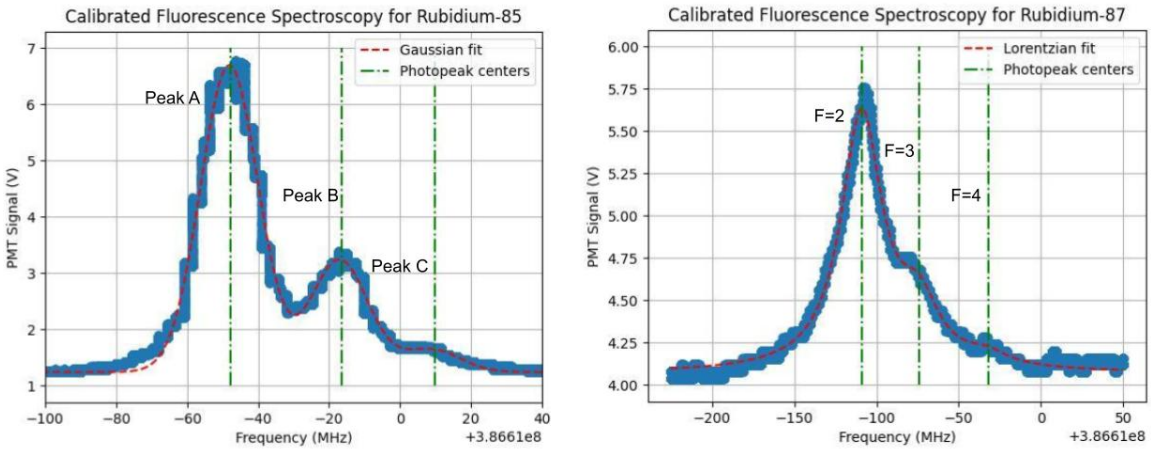

Figure 4.6: Graphs of $5D_{5/2}$ fluorescence spectroscopy data for rubidium-85 (left) and rubidium-87 (right), plotting PMT fluorescence signal vs. converted frequency scale. On the y-axis, 10mV corresponds to 1 photon. Red dashed line is the fit of the data (Gaussian for ^{85}Rb and Lorentzian for ^{87}Rb); green dashed lines signify the central values of each photopeak found using the fits.

in megahertz (see Figure 4.6).

The exact measurement of the wavelengths using the wavemeter were not accurate, as the wavemeter had an unknown offset to its measurements. Thus, determining the exact wavelengths of the hyperfine structure transitions in this manner was likely to be unfruitful. However, the wavelength differences corresponding to differences in the piezo voltages were much more likely to be correct. This means that while we could not find the precise transition wavelengths, we could find the splittings of the hyperfine structure.

The central values and splittings of the photopeaks were determined by fitting the data to the sum of three Gaussian functions for ^{87}Rb (Equation 4.4, where A is peak amplitude, x_o is peak position, and d is peak width) and the sum of three Lorentzian functions (Equation 3.1) for ^{85}Rb - one for each of the three observed photopeaks. The wider peaks and longer tails of the ^{87}Rb spectrum made it more suitable to a Lorentzian fit, but since the ^{85}Rb spectrum had significantly shorter tails, it could be

fit with a Gaussian function.

$$Ae^{\frac{-(x-x_o)^2}{2d^2}} \tag{4.4}$$

The ^{87}Rb spectrum was fit with a sum of Gaussian functions such that the x_o position parameter, for the smaller/second two peaks, was composed of a sum of the x_o parameter for the first peak and a Δx_o parameter that was different for each peak ($x_o+\Delta x_{oa}$ and $x_o+\Delta x_{ob}$). The measured splittings stem from the Δx_o parameters and can be seen in Table 1.2. Additionally, the d (peak width) parameter was held constant for all fluorescence peaks, as they did not vary greatly in width.

The ^{85}Rb spectrum was fit with a sum of Lorentzian functions where the x_o position parameter for the smaller two peaks was a sum of the initial x_o parameter and Δx_o parameters. However, contrasting the ^{87}Rb spectrum fit, the smallest/rightmost spectral peak's position parameter sum also included the Δx_o term from the middle peak ($x_o+\Delta x_{oa}+\Delta x_{ob}$). The splittings obtained from the Δx_o terms can also be found in Table 1.2. Similar to the ^{87}Rb fit, the d (width) parameter was held constant for all three peaks.

Observed $5D_{5/2}$ Splitting Frequencies (MHz)			
Rubidium-85		Rubidium-87	
Peak A → Peak B	31.0 ± 4.7 MHz	F=2 → F=3	34.6 ± 75.8* MHz
Peak B → Peak C	25.9 ± 22.2* MHz	F=3 → F=3	41.8 ± 196.6* MHz

Table 1.2: Observed hyperfine structure splittings for $5D_{5/2}$ levels of rubidium-85 and rubidium-87 in megahertz. F levels for ^{85}Rb splittings are currently uncertain, and are instead labeled by Peaks A, B, and C. Starred error bars are larger than expected; more analysis and data are likely needed.

The known literature values for the ^{87}Rb 5D hyperfine splittings are 22.9 MHz and 28.8 MHz [10] (compared to the experimental values of 34.6 and 41.8 MHz, respectively). These are the splittings for the F=2→F=3 and F=3→F=4 transitions.

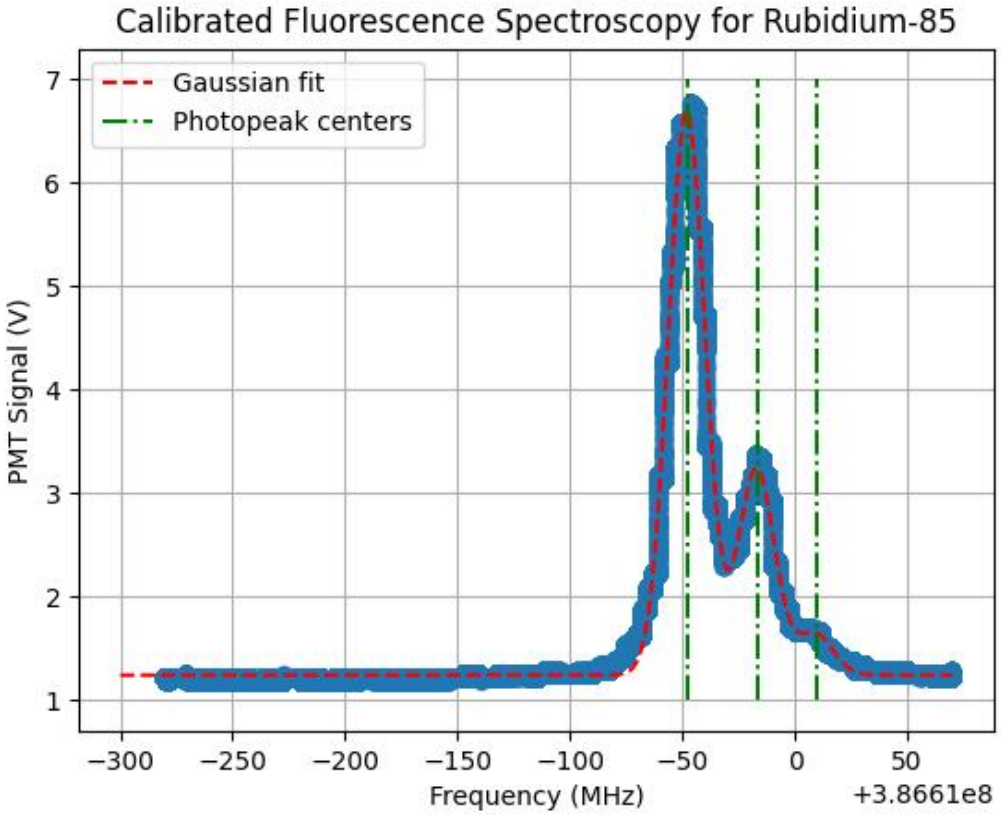

Figure 4.7: Graph of $5D_{5/2}$ fluorescence spectroscopy data for rubidium-85, showing the full range of data used to generate the Gaussian fit (including a long background).

There is an approximately 12 MHz difference between both sets of experimental and literature values for the splittings. This 12 MHz offset between known and experimental values should be further analyzed during the future of this research.

4.1.1 Error Analysis

The errors seen on the splittings in Table 1.2 notably appear to be larger than reasonable. For example, looking at the ^{87}Rb spectrum in Figure 4.6, I could visually approximate the error on the smallest, rightmost peak (F=4) to be approximately ±25 MHz, at most. However, the error in Table 1.2 is nearly 200 MHZ. These errors

were given by Python's $curve\_fit()$ function, and it is assumed that an unknown flaw in the math or code determining the errors caused them to be larger than expected. After realizing this, several steps were taken to reduce the error being given by the code, including:

- Using different fit functions on the data (Gaussian vs. Lorentzian). A Gaussian fit reduced the error for the ^{85}Rb spectrum, but not the ^{87}Rb spectrum.
- Including more of the data set to obtain a larger background, particularly for the ^{85}Rb spectrum, as seen in Figure 4.7.
- Holding the d (peak width) parameter constant for all photopeaks.
- Using different numbers of Δx_o terms for the rightmost peak - two Δx_o terms decreased the error on the ^{87}Rb spectrum, but not the ^{85}Rb spectrum.
- Changing the applied errorbars from the square root of the number of photon counts of the data to the square root of the photon counts from exclusively the background. The large number of counts on the highest peak likely overpowered the error data and caused greater error on the smaller peaks.

The error given by the code was decreased significantly through these processes, but not to a reasonable amount. After attempting the above methods, a second method of determining the initially applied errorbars was attempted. In this method, I focused only on the ^{85}Rb spectrum, as it had the cleanest data. I looked at the residuals of the ^{85}Rb spectrum fit (which can be seen in Figure 4.8), took the standard deviation of the residuals about significant features in the data (the background and each of the three photopeaks), and set those standard deviations to be the initially applied errorbars in the Python code. Unfortunately, this method instead generated the opposite problem - the errorbars returned by the code were now unreasonably

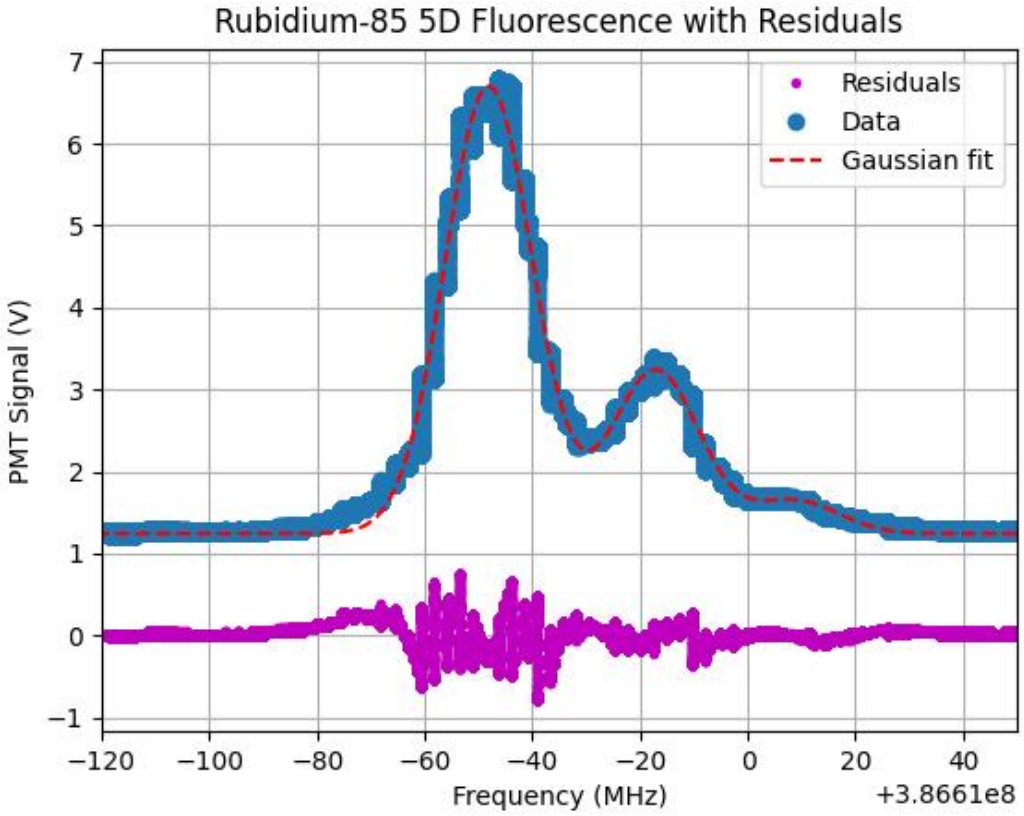

Figure 4.8: Graph of $5D_{5/2}$ fluorescence spectroscopy data for rubidium-85 including residuals of the fit, in pink.

small (on the order of 0.001 MHz) instead of unreasonably large. However, this method also caused the fit to find slightly different photopeaks compared to when the error was the photon counts. In an alternative analysis of the hyperfine splitting data, values of the splittings found by both methods of errorbar generation were averaged and can be seen in Table 4.1, with the error being the difference between them. However, to decrease the error further, more data should be taken, with an effort to acquire more background data and thinner photopeaks.

Average Values for ^{85}Rb 5D Hyperfine Splittings	
Peak A $\rightarrow$ Peak B	31.02 $\pm$ 0.02 MHz
Peak B $\rightarrow$ Peak C	26.0 $\pm$ 0.1 MHz

Table 4.1: 5D hyperfine splittings for $5D_{5/2}$ levels of rubidium-85 in megahertz, averaged from two methods of errorbar generation (square root of photon counts vs. standard deviation of residuals).

Figure 4.9: Photograph of the MOT fluorescing blue, taken by students in the lab of Dr. Seth Aubin.

4.2 5D Fluorescence in Cold Atom Apparatus

Fluorescence of the MOT in the cold atom apparatus was successfully observed by William Miyahira and myself just after winter break, using the resonant frequency found in the vapor cell. Unlike in the vapor cell, where fluorescence was not visible to the naked eye, fluorescence of the MOT could be visibly seen, both with the eye and with a regular phone camera (see Figure 4.9).

We observed the $5D_{5/2}$ hyperfine levels of rubidium-87 as three photopeaks in the

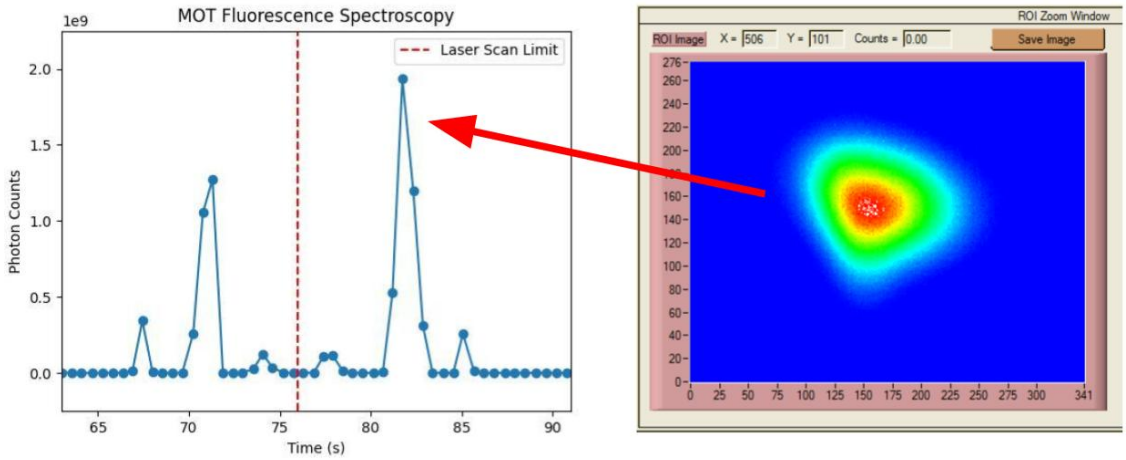

Figure 4.10: Left side depicts photon count vs. time (frequency) data for fluorescence spectroscopy of the MOT. Blue connecting lines are for visual aid and do not indicate interpolation. Laser frequency scan pivots and goes from increasing to decreasing about red dashed line; both sets of three photopeaks on either side occur at the same frequencies. Right side depicts photodetector data from MOT and shows visible fluorescence corresponding to strongest photopeak (see red arrow).

fluorescence of the MOT (see Figure 4.10). The exact strength of the photopeaks varied over time due to the population of atoms within the MOT decreasing with time (or increasing, if the population decreased too much and needed to be added to). However, the relative strength between the three photopeaks was consistent, with two smaller peaks and one larger one. This relative strength could be observed visually, with the largest photopeak fluorescing visually brighter than the other two photopeaks. Additionally, the spacing (or hyperfine splittings) between photopeaks appeared relatively consistent. With further research, the time-scale x-axis of this data could likely be calibrated and converted to a wavelength/frequency scale, allowing us to determine the exact values of the hyperfine splittings of $5D_{5/2}$ levels of rubidium-87 in the MOT.

Compared to the fluorescence spectroscopy observed in a vapor cell for the $5D_{5/2}$ hyperfine structure of ^{87}Rb (in that section's second iteration, as in Figure 4.6), the

fluorescence spectroscopy observed in the MOT had much thinner photopeaks. Additionally, the relative strength of the three photopeaks differed between the vapor cell and the MOT, which could be impacted by the different input laser polarizations in each setup. However, from a visual standpoint, the splittings between each photopeak in the MOT appeared to be relatively similar to those observed in the vapor cell (see Figure 4.6). The ratio of the splittings in the MOT (found by approximating the time-scale splittings on the x-axis) is approximately 1.3, and the ratio of the splittings from the ^{87}Rb data in the vapor cell is approximately 1.2. This speaks to the relative accuracy of the measurements of the splittings; however, converting the time axis of the data from the MOT into frequency is necessary to confirm the similarities or differences between the two sets of measurements.

Chapter 5

Conclusion & Next Steps

A main goal of this research was to determine the frequency values of the transition from the 5P to 5D levels of rubidium. I was successful in determining the transition value to the $5D_{5/2}$ level to be 775.9776 nm (as seen in Table 1.1), as measured using a wavemeter. This value and the spectroscopic methods used to obtain it can be replicated and used in future research to easily and efficiently excite rubidium to the $5D_{5/2}$ level.

A second goal of this research was to measure the hyperfine splittings of rubidium's 5D levels. I measured the $5D_{5/2}$ hyperfine splittings of rubidium-85 and rubidium-87 in a vapor cell, as seen in Table 1.2 and Figure 4.6. I also observed the $5D_{5/2}$ hyperfine splittings of rubidium-87 in a cold atom apparatus. More research is needed to analyze the accuracy of these values and reassess the error on them; however, both the spectroscopic method used to measure them and the fitting equations used to convert the time-scale data to wavelength- and frequency-scale data (such as Equation 4.1) can be used in future work measuring the splittings of other hyperfine structures, such as those of the $5D_{3/2}$ level.

Further work on this research could include determining the transition wavelength from the 5P levels up to the $5D_{3/2}$ levels, which should be relatively easy using the experimental setup I created. More data should also be taken for the $5D_{5/2}$ levels in

order to decrease the measured error on the hyperfine splittings, with a particular focus on decreasing the width of the photopeaks and obtaining more measurements of the background. The hyperfine structure data from the vapor cell should also be analyzed more to assess the accuracy of the hyperfine splitting values, including the error values and the apparent offset from the known literature values of the splittings, as well as to determine the F levels of the $5D_{5/2}$ splittings of rubidium-85. The time axis of the observations from the cold atom apparatus could also be calibrated and converted to frequency, which would ultimately allow for a better comparison between the hyperfine structure observed in a vapor cell and in the MOT.

This research will ultimately be used to efficiently excite rubidium atoms up to and through the 5D levels to reach the Rydberg levels. By utilizing the transition frequency value that I determined as well as the experimental setup I created to observe this transition and its structure, it will be much easier for future researchers to excite rubidium to the Rydberg levels. In conclusion, the work in this thesis will aid the research being done to use rubidium atoms in the Rydberg levels as indirect detectors of electrons and other charged particles.

References

[1] Catherine Sturner. "Development of a 780 nm external cavity diode laser for rubidium spectroscopy". B.Sc. Thesis (unpublished). College of William & Mary, 2023.

[2] Adela Marian. "Direct Frequency Comb Spectroscopy for Optical Frequency Metrology and Coherent Interactions". PhD thesis. University of Colorado Boulder, 2005. URL: https://jila.colorado.edu/bibcite/reference/12239.

[3] Aubin, S. and Pegahan, S. and DeStefano, N. C. and Behary, R. and Averett, T. D. and Mikhailov, E. E. and Novikova, I. B. and Ramaswamy, A. and Malinovskaya, S. and Camsonne, A. and Park, G. and and Zhang, S. *Development of a Rydberg Atom-based Apparatus for Tracking Charged Particles*. presented at 54th Annual Meeting of the APS Division of Atomic, Molecular and Optical Physics, Spokane, Washington. 2023.

[4] Donald P. Fahey and Michael W. Noel. "Excitation of Rydberg states in rubidium with near infrared diode lasers". In: *Opt. Express* 19.18 (Aug. 2011), pp. 17002–17012. DOI: 10.1364/OE.19.017002. URL: https://opg.optica.org/oe/abstract.cfm?URI=oe-19-18-17002.

[5] Georg Raithel. *Rydberg atoms in fundamental physics and quantum-technology applications*. Physics Colloquium. Department of Physics, College of William Mary, Oct. 2024.

[6] John S. Townsend. *A modem approach to quantum mechanics*. University Science Books, 2012. ISBN: 978-1-891389-78-8.

[7] Daryl W. Preston. "Doppler-free saturated absorption: Laser spectroscopy". In: *American Journal of Physics* 64.11 (Nov. 1996), pp. 1432–1436. ISSN: 0002-9505. DOI: 10.1119/1.18457. eprint: https://pubs.aip.org/aapt/ajp/article-pdf/64/11/1432/11979448/1432_1_online.pdf. URL: https://doi.org/10.1119/1.18457.

[8] Ran Finkelstein et al. "A practical guide to electromagnetically induced transparency in atomic vapor". In: *New Journal of Physics* 25.3 (Mar. 2023), p. 035001. DOI: 10.1088/1367-2630/acbc40. URL: https://dx.doi.org/10.1088/1367-2630/acbc40.

[9] Daniel A. Steck. *Rubidium 85 D Line Data*. May 2024. URL: https://steck.us/alkalidata/.

[10] Daniel A. Steck. *Rubidium 87 D Line Data*. May 2024. URL: https://steck.us/alkalidata/.

[11] Bureau International des Poids et Mesures. *Standard frequency: 385 THz (778 nm) – 85Rb*. BIPM Document. 2005. URL: https://www.bipm.org/en/search?p_p_id=search_portlet&p_p_lifecycle=2&p_p_state=normal&p_p_mode=view&p_p_resource_id=%2Fdownload%2Fpublication&p_p_cacheability=cacheLevelPage&_search_portlet_dlFileId=41549390&_search_portlet_priv_r_p_javax.portlet.action=search&_search_portlet_priv_r_p_source=BIPM&_search_portlet_priv_r_p_p_p_lifecycle=1&_search_portlet_priv_r_p_formDate=1729267641669&_search_portlet_priv_r_p_query=rubidium+778.